1-1-1982

Variability of K due to residual stresses.

Lung-Hen Chow

VARIABILITY OF K DUE TO RESIDUAL STRESSES

by

Lung-Hen Chow

A Thesis

Presented to the Graduate Committee

of Lehigh University

in Candidacy for the Degree of

Master of Science

in

Mechanical Engineering and Mechanics

Lehigh University

1982

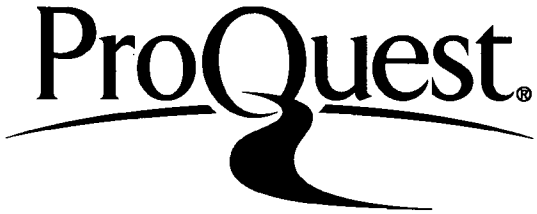

CERTIFICATE OF APPROVAL

This thesis is accepted and approved in partial fulfillment of the requirements for the degree of Master of Science.

May 5/82
date

Professor in Charge

Chairman of Department

ACKNOWLEDGEMENTS

The author wishes to express his sincere thanks to his advisor, Professor R. Roberts, for his encouragement through the course of this research. His guidance and helpful criticism in this work is highly appreciated.

Appreciation is also expressed to Mrs. Donna Reiss for her help in typing the manuscript.

TABLE OF CONTENTS

LIST OF FIGURES

LIST OF TABLES

ABSTRACT:

It is well known that such factors as stress range, stress concentration and initial flaw condition are very important in the development of fatigue cracks and the fatigue life of a large welded structure such as a welded bridge member. In general, the plates which are assembled into bridges are flame-cut and the welded details are not stress relieved. This produces a rather complex residual stress pattern in the regions where the fatigue cracks form and propagate. Thus, when investigating the fatigue life or fracture response of such members, it is important to understand how residual stresses affect their behavior.

In general, the residual stresses are caused by the web-to-flange welds, the flame-cut plate edges on the nominal section of the welded beam, and the local weld details.

For convenience, an edge-crack model was used to simplify the calculation of the stress intensity factor, K. Using this idealized model the stress intensity factor for several stress distributions were calculated. Superposition was then used to estimate the effect of the residual stress field on the K value. The results obtained show that the residual stresses can have a large effect of the calculation of K.

NOMENCLATURE:

K = stress intensity factor, ksi$\sqrt{in}$ *

K_I = stress intensity factor in Mode I, ksi$\sqrt{in}$

K_C = critical stress intensity factor subjected to fracture, ksi$\sqrt{in}$

a = edge-crack size of the specimen, in $

b = the length of residual stress block, in

σ = nominal stress level, ksi x.

σ_{rs} = residual stress, ksi .

σ_c = uniform residual stress, ksi .

σ_{max} = maximum stress, ksi

E = Young's modulus, ksi .

---

* 1.0 ksi$\sqrt{in}$ = 1.0998 MN/m$^{3/2}$

$ 1.0 in = 25.4 mm

x 1.0 ksi = 6.90 MPa

1. INTRODUCTION:

It is known that residual stresses will occur in a weld and welded structures when the dimensional changes caused by heating and cooling cannot take place freely. It is also known that these residual stresses can have a large adverse effect on stress-corrosion behavior, corrosion fatigue, and fracture behavior.

Fracture Mechanics uses a single parameter[12]*, K, the stress intensity factor to characterize the stress field ahead of a sharp crack. This parameter is related to both the nominal stress level, σ, and the size of the crack, a, in the structural member. It will be assumed in the analysis presented here that superposition[1] can be used to calculate the effect of residual stress on K values. Thus, the residual stresses will be treated in a manner similar to the nominal stresses in the calculation of K.

Because of the difficulty of measuring residual stress inside structural members, it is impossible to describe precise values of residual stress at a weldment. Only average values of the residual stress can be ascribed to the details.

---

* the number inside the bracket represents the reference number in REFERENCES

It is these average values that will be used to calculate the K values. Thus, in this paper, several simple residual stress patterns are used to examine how they influence the calculation of K.

2. MEASUREMENTS OF RESIDUAL STRESSES IN WELDMENT:

As mentioned before, it is not easy to measure the magnitude of residual stress. It is only possible from a practical standpoint to obtain average values of the distributions. To obtain these values, the method of sectioning[5,6] can be used to determine the nominal section residual stress pattern in typical welded beams and rolled beams. The hole drilling method[7] can be used to determine the residual stresses local to the welded details.

The method of sectioning is based on the principle that the internal stresses in the beam are relieved by slicing the beam into small strips (Fig. 1,2). The residual stress in each strip can be assessed by measuring the length of strips before and after slicing with a mechanical strain gage. The residual stress at the measured surface can be calculated by Hooke's law,

$$\sigma_{rs} = \frac{-E}{L} (\Delta L) \qquad (1)$$

where L is gage length, E is modulus in elasticity and ΔL is

positive for an increase of length, σ_{rs} is positive for a tensile residual stress.

The hole drilling method is based on the principle that drilling a hole in a stress field disturbs the stress equilibrium, and returning the disturbed stress field to the equilibrium results in deformations of the surface close to the hole. Bonded electrical strain gages are mounted in 45^{o} strain rosette to measure these surface deformations. The direction and magnitude of principal residual stresses thus can be calculated[8]. The gage and stress field orientation is shown in Figure 3.

Some test results for residual stress distributions are shown[1,5,6] in Figures 4 to 19. The three specimens are fabricated from flame-cut plates, A36, A588, A514, in groove welds shown in Figs. 4 to 6. All three curves show relatively high tensile stresses at the flange tips of the specimens made of flame-cut plates, and very high tensile stresses in the central weld region. Because of their similar distributions, we may conclude that there is no great influence caused by different type of steel on residual stresses in large and heavy shapes. This evidence can also be seen in Figs. 7 and 8 for beams 12H79, 14H202 which are oxygen-cut

A36 plates. The other four 15H290 flame-cut plates of A36 steel and A441 steel with fillet and groove welds shown in Figs. 9 and 12 show similar distributions to the preceeding figures. As may be observed from these distributions, there are steep gradients in the weld region and at the flame-cut edges.

Figures 13 through 16 show the residual stresses as measured in the four 15H290 specimens fabricated from universal-mill plates. Each specimen made of universal-mill plate corresponds to a similar specimen made of flame-cut plates (Figs. 9 to 12) as such the distributions may be compared directly. Instead of very high tensile stresses as in the flame-cut plates, there are high compressive stresses at the flange tips of the shapes made of universal-mill plates.

Figures 17, 18 and 19 show residual stresses in hot-rolled shapes for W36 x 2360 A36 steel, W36 x 230 A588 steel and 14 W426 A7 steel. As in the welded shape 15H290 made of universal-mill plates, there are similar distributions at the flange tip and the region of web-to-flange.

3. ANALYTICAL MODELING:

From experimental measurements of residual stresses in full-size structures shown in figures 4 to 19, it can be

concluded there will be high steep residual stress distributions at the flame-cut and hot-rolled edges, in the region of web-to-flange, and in the welded areas. In the other regions the residual stress distributions are much smoother.

To understand the role residual stresses play in the behavior of K, the residual stresses will be modeled by a series of residual stress distributions. These residual stress patterns contain first-order linearly increasing and decreasing curves, second-order continuously increasing and decreasing curves, and isosceles-triangular distribution etc., shown in Figure 20. They are all based upon the same total force along the crack-line in order to facilitate comparisons of the results on K behavior. These stress patterns together with the method of superposition will be enough to fit real residual stress distribution as shown in Figures 4 through 19.

3.1 Derivation of K Due to Basic Residual Stress Patterns

The stress-intensity factor can be expressed in the form

$$K = F(g) \cdot \sigma \cdot \sqrt{a} \qquad (2)$$

where F(g) is dependent on the specimen and crack geometry. Various stress intensity factor equations for different geometries and loading conditions have been published[2,3,4].

The stress intensity factor equation for a semi-infinite single edge crack subjected to a concentrated force P, per unit thickness, is given by[3]

$$K_I = \frac{2P}{\sqrt{\pi a}} \frac{F(b/a)}{\sqrt{1-(b/a)^2}} \qquad (3)$$

in which a is crack length, b is distance from the edge of the plate to which P is acting on. F(b/a) shown in Fig. 21, which is a parameter dependent upon b/a, ranges from 1.30 to 1.0 as b/a from 0 to 1.

By taking advantage of equation (3), together with numerical integration and the superposition method, we can derive stress-intensity factors for each residual stress pattern of Figure 20, and obtain numerical values of each pattern as b/a ranges from 0 to 1. The following are their derivations.

(A) The case of uniform tensile residual stress

$$\sigma = \sigma_c = \text{constant}$$

First, the concentrated load P in equation (3) can be replaced by ΔP and integrated from 0 to b. Hence, we have $\Delta P = \sigma \Delta b$. Thus, in this case, $\Delta P = \sigma c \Delta b$, that is, $dP = \sigma_c db$.

$$K1 = \int_0^b \frac{2\sigma_c db}{\sqrt{\pi a}} \frac{F(b/a)}{\sqrt{1-(b/a)^2}}$$

$$= \frac{2\sigma_c a}{\sqrt{\pi a}} \int_0^{b/a} \frac{F(b/a)}{\sqrt{1-(b/a)^2}} d(b/a)$$

$$= \frac{2\sigma c}{\pi} \sqrt{\pi a} \int_0^{\sin^{-1}b/a} F(b/a) d(\sin^{-1}b/a)$$

$$= [F(b/a)\sin^{-1}(b/a) - \int_{F(o)}^{F(b/a)} \sin^{-1}(b/a) dF(b/a)] \frac{2\sigma c}{\pi} \sqrt{\pi a}$$

$$\therefore K1(b/a) = \frac{2\sigma c}{\pi} \sqrt{\pi a} \sin^{-1}b/a \; FA(b/a)$$

where $FA(b/a) = [F(b/a) - \frac{1}{\sin^{-1}b/a} \int_{F(o)}^{F(b/a)} \sin^{-1}b/a \; dF(b/a)]$

By numerical integration, the FA(b/a) with respect to b/a through 0 to 1 can be calculated. These results are shown in Figure 22.

(B) The case of first-order increasing residual stress

$$\sigma = 2\sigma_c x/b \qquad 0 \leq x \leq b$$

where $1/2(2\sigma c)b = \sigma cb$ = constant is the same force as case (A). Similarly, we have

$$K2 = \int_0^b \frac{2\sigma dx}{\sqrt{\pi a}} \frac{F(x/a)}{\sqrt{1-(x/a)^2}}$$

$$= \int_0^b \frac{2(2\sigma_c x/b)dx}{\sqrt{\pi a}} \frac{F(x/a)}{\sqrt{1-(x/a)^2}}$$

$$= \frac{4\sigma_c a^2}{b\sqrt{\pi a}} \int_0^{b/a} \left[\frac{(x/a)d(x/a)}{\sqrt{1-(x/a)^2}} \right] F(x/a)$$

$$= \frac{4\sigma_c}{\pi} \frac{\sqrt{\pi a}}{b/a} \int_0^{b/a} -F(x/a)d(\sqrt{1-(x/a)^2})$$

$$\therefore K_2(b/a) = \frac{4\sigma_c}{\pi} \frac{\sqrt{\pi a}}{b/a} FB(b/a)$$

where $FB(b/a) = F(0)-F(b/a)\sqrt{1-(b/a)^2} + \int_0^{b/a} \sqrt{1-(x/a)^2}\, dF(x/a)$

and $F(0) = 1.30$

The numerical values of FB(b/a) are calculated and plotted in Figure 22 as a function of b/a from 0 to 1.

(C) The case of second-order continuously increasing concave residual stress

$$\sigma = 3\sigma_c(x/b)^2 \qquad 0 \leq x \leq b$$

in which has also the same total force with Case (A).

Then,

$$K3 = \int_0^b \frac{2\sigma dx}{\sqrt{\pi a}} \frac{F(x/a)}{\sqrt{1-(x/a)^2}}$$

$$= \int_0^b \frac{2(3\sigma_c x^2/b^2)dx}{\sqrt{\pi a}} \frac{F(x/a)}{\sqrt{1-(x/a)^2}}$$

$$= \frac{6\sigma_c}{\pi} \frac{\sqrt{\pi a}}{(b/a)^2} \int_0^{b/a} \left[\frac{(x/a)^2 d(x/a)}{\sqrt{1-(x/a)^2}} \right] F(x/a)$$

$$= \frac{6\sigma_c}{\pi} \frac{\sqrt{\pi a}}{(b/a)^2} \int_0^{b/a} F(x/a) d\left[-\frac{1}{2} \frac{x}{a} \sqrt{1-(x/a)^2} + \frac{1}{2} \sin^{-1} \frac{x}{a} \right]$$

$$\therefore K3(b/a) = \frac{6\sigma_c}{\pi} \frac{\sqrt{\pi a}}{(b/a)^2} FC(b/a)$$

where

$$FC(b/a) = \frac{1}{2} F(b/a) \left[-\frac{b}{a} \sqrt{1-(b/a)^2} + \sin^{-1} \frac{b}{a} \right]$$

$$- \int_0^{b/a} \frac{1}{2} \left[\sin^{-1} \frac{x}{a} - \frac{x}{a} \sqrt{1-(x/a)^2} \right] dF(x/a)$$

The numerical values of FC(b/a) are calculated and plotted in Figure 22 for b/a from 0 to 1.

For comparative purposes, let K1, K2 and K3 are as shown below.

$$K1(b/a) = \frac{\sigma_c\sqrt{\pi a}}{\pi(b/a)^2}\, F1(b/a)$$

$$K2(b/a) = \frac{\sigma_c\sqrt{\pi}}{\pi(b/a)^2}\, F2(b/a)$$

$$K3(b/a) = \frac{\sigma_c\sqrt{\pi a}}{\pi(b/a)^2}\, F3(b/a)$$

where

$$F1(b/a) = 2(b/a)^2 \sin^{-1}b/a\, FA(b/a)$$

$$F2(b/a) = 4(b/a)\, FB(b/a)$$

$$F3(b/a) = 6FC(b/a)$$

(4)

(D) The case of first-order decreasing residual stress

$$\sigma = 2\sigma_c(1-x/b) = 2\sigma_c - 2\sigma_c x/b \qquad 0 \le x \le b$$

$$\therefore K4 = \int_0^b \frac{2[2\sigma_c - 2\sigma_c x/b]dx}{\sqrt{\pi a}} \frac{F(x/a)}{\sqrt{1-(x/a)^2}}$$

$$= 2\int_0^b \frac{2\sigma_c dx}{\sqrt{\pi a}} \frac{F(x/a)}{\sqrt{1-(x/a)^2}} - \int_0^b \frac{2(2\sigma_c x/b)dx}{\sqrt{\pi a}} \frac{F(x/a)}{\sqrt{1-(x/a)^2}}$$

$$= 2K_1(b/a) - K2(b/a)$$

Since K1(b/a) and K2(b/a) have been obtained in equation (4), numerical values of K4(b/a) for $0 < b/a < 1$ are readily

calculated.

$$K4(b/a) = \frac{\sigma_c\sqrt{\pi a}}{\pi(b/a)^2}\, F4(b/a)$$

where $F4(b/a) = 2F1(b/a) - F2(b/a)$ (5)

(E) The case of second-order continuously decreasing concave residual stress

$$\sigma = 3\sigma_c(1-x/b)^2 = 3\sigma_c(x/b)^2 - 3(2\sigma_c x/b) + 3\sigma_c$$

By the method of superposition,

$$K5 = \int_0^b \frac{2[3\sigma_c(1-x/b)^2]dx}{\sqrt{\pi a}} \frac{F(x/a)}{\sqrt{1-(x/a)^2}}$$

$$= \int_0^b \frac{2(3\sigma_c x^2/b^2)dx}{\sqrt{\pi a}} \frac{F(x/a)}{\sqrt{1-(x/a)^2}} - 3\int_0^b \frac{2(2\sigma_c x/b)dx}{\sqrt{\pi a}} \frac{F(x/a)}{\sqrt{1-(x/a)^2}}$$

$$+ 3\int_0^b \frac{2\sigma_c dx}{\sqrt{\pi a}} \frac{F(x/a)}{\sqrt{1-(x/a)^2}}$$

$$= K3(b/a) - 3K2(b/a) + 3K1(b/a)$$

$$\therefore K5(b/a) = \frac{\sigma_c\sqrt{\pi a}}{\pi(b/a)^2}\, F5(b/a)$$

where $F5(b/a) = F3(b/a) - 3F2(b/a) + 3F1(b/a)$ (6)

(F) The case of isosceles-triangular residual stress

$$\sigma = \begin{cases} 2\sigma_c(2x/b) & 0 \le x \le b/2 \\ 2\sigma_c(2-2x/b) & b/2 \le x \le b \end{cases}$$

Then,

$$K6 = \int_0^{b/2} \frac{8\sigma_c(x/b)dx}{\sqrt{\pi a}} \frac{F(x/a)}{\sqrt{1-(x/a)^2}} + \int_{b/2}^{b} \frac{[8\sigma_c - 8\sigma_c(x/b)]dx}{\sqrt{\pi a}} \frac{F(x/a)}{\sqrt{1-(x/a)^2}}$$

$$= 2\int_0^{b} \frac{2[2\sigma_c - 2\sigma_c x/b]dx}{\sqrt{\pi a}} \frac{F(x/a)}{\sqrt{1-(x/a)^2}} + 2\int_0^{b/2} \frac{2[2\sigma_c(x/b/2)]dx}{\sqrt{\pi a}} \frac{F(x/a)}{\sqrt{1-(x/a)^2}}$$

$$- 4\int_0^{b/2} \frac{2\sigma_c dx}{\sqrt{\pi a}} \frac{F(x/a)}{\sqrt{1-(x/a)^2}}$$

$$= 2K4(b/a) + 2K2(b/2a) - 4K1(b/2a)$$

$$= 2[\frac{\sigma_c\sqrt{\pi a}}{\pi(b/a)^2}]F4(b/a) + 2[\frac{\sigma_c\sqrt{\pi a}}{\pi(b/2a)^2}]F2(b/2a) - 4[\frac{\sigma_c\sqrt{\pi a}}{\pi(b/2a)^2}]F1(\frac{b}{2a})$$

$$= \frac{\sigma_c\sqrt{\pi a}}{\pi(b/a)^2}\,[2F_4(b/a) + 8F_2(b/2a) - 16F_1(b/2a)]$$

$$\therefore K6(b/a) = \frac{\sigma_c\sqrt{\pi a}}{\pi(b/a)^2} F6(b/a) \qquad (7)$$

where $F6(b/a) = 2F4(b/a) + 8F2(b/2a) - 16F1(b/2a)$

(G) The case of second-order continuously increasing convex residual stress

$$\sigma = 1.5\sigma_c[1-(1-x/b)^2] = 1.5\sigma_c[2(x/b) - (x/b)^2] \quad 0 \leq x \leq b$$

and the total force along the crack-line is also σcb, that is, $2/3\ (1.5\sigma_c)b = \sigma_c b$ = constant.

Then,

$$K_7 = \int_0^b \frac{2\{1.5\sigma_c[2(x/b)-(x/b)^2]\}dx}{\sqrt{\pi a}} \frac{F(x/a)}{\sqrt{1-(x/a)^2}}$$

$$= 1.5\int_0^b \frac{2(2\sigma_c x/b)dx}{\sqrt{\pi a}} \frac{F(x/a)}{\sqrt{1-(x/a)^2}} - 0.5\int_0^b \frac{2(3\sigma_c x^2/b^2)dx}{\sqrt{\pi a}} \frac{F(x/a)}{\sqrt{1-(x/a)^2}}$$

$$= 1.5\ K_2(b/a) - 0.5K_3(b/a)$$

$$\therefore K_7(b/a) = \frac{\sigma_c\sqrt{\pi a}}{\pi(b/a)^2} F_7(b/a) \qquad (8)$$

where $F7(b/a) = 1.5F2(b/a) - 0.5F3(b/a)$

(H) The case of second-order continuously decreasing convex residual stress

$$\sigma = 1.5\sigma_c\ [1-(x/b)^2] \qquad 0 \leq x \leq b$$

Then,

$$K_8 = \int_0^b \frac{2\{1.5\sigma_c[1-(x/b)^2]\}dx}{\sqrt{\pi a}} \frac{F(x/a)}{\sqrt{1-(x/a)^2}}$$

$$= 1.5\int_0^b \frac{2\sigma_c dx}{\sqrt{\pi a}} \frac{F(x/a)}{\sqrt{1-(x/a)^2}} - 0.5\int_0^b \frac{2(3\sigma_c x^2/b^2)dx}{\sqrt{\pi a}} \frac{F(x/a)}{\sqrt{1-(x/a)^2}}$$

$$= 1.5\ K_1(b/a) - 0.5\ K_3(b/a)$$

$$K_8(b/a) = \frac{\sigma_c\sqrt{\pi a}}{\pi(b/a)^2}\ F_8(b/a)$$

where $F_8(b/a) = 1.5\ F_1(b/a) - 0.5\ F_3(b/a)$.

(I) The case of parabolic distributed residual stress

$$\sigma = 1.5\sigma_c\ [1-(\frac{x-b/2}{b/2})^2]$$

$$= 1.5\sigma_c\ [4(x/b) - 4(x/b)^2]$$

$$= 6\sigma_c\ [(x/b) - (x/b)^2] \qquad 0 \leq x \leq b$$

Then,

$$K_9 = \int_0^b \frac{2\{6\sigma_c[(x/b)-(x/b)^2]\}dx}{\sqrt{\pi a}} \frac{F(x/a)}{\sqrt{1-(x/a)^2}}$$

$$= 3\int_0^b \frac{2(2\sigma_c x/b)dx}{\sqrt{\pi a}} \frac{F(x/a)}{\sqrt{1-(x/a)^2}} - 2\int_0^b \frac{2(3\sigma_c x^2/b^2)dx}{\sqrt{\pi a}} \frac{F(x/a)}{\sqrt{1-(x/a)^2}}$$

$$= 3K2(b/a)-2K3(b/a)$$

$$\therefore K9(b/a) = \frac{\sigma_c\sqrt{\pi a}}{\pi(b/a)^2} F9(b/a) \qquad (9)$$

where $F9(b/a) = 3F2(b/a) - 2F3(b/a)$

F1, F2, F3, F4, F5, F6, F7, F8 and F9 corresponding to K1, K2, K3, K4, K5, K6, K7, K8 and K9 are tabulated in Table 1 for b/a from 0 to 1.

3.2 Special Cases Derived from Basic Residual Stress Patterns

It cannot be expected that by use of only one of the preceding stress patterns the whole real residual stress distributions can be modeled. However, proper use of the given results can be used to determine K for complex stress patterns.

The following are two examples.

(a) The combination of Case (A) and Case (B)

Residual stress distribution for this combination is shown in Figure 23. Based on the same total force, $\sigma_c b$,

$$(e\sigma_c)b + \frac{1}{2}\sigma_{max}b = \sigma_c b = \text{constant}$$

$$\therefore \sigma_{max} = 2(1-e)\sigma_c$$

$$\sigma = e\sigma_c + \sigma_{max}\, x/b = e\sigma_c + 2(1-e)\sigma_c\, x/b \quad 0 \leq x \leq b$$

where $e\sigma_c$ = the residual stress at the edge of plate

σ_{max} = maximum residual stress along the crack-line due to case (B)

Thus, the stress-intensity factor equation is given by use of equation (3)

$$K = \int_0^b \frac{2\sigma dx}{\sqrt{\pi a}} \frac{F(x/a)}{\sqrt{1-(x/a)^2}}$$

$$= \int_0^b \frac{2[e\sigma_c + 2(1-e)\sigma_c x/b]dx}{\sqrt{\pi a}} \frac{F(x/a)}{\sqrt{1-(x/a)^2}}$$

$$= eK1(b/a) + (1-e)K2(b/a) \qquad (10)$$

Note that

$K = 2K1(b/a) - K2(b/a) = K4(b/a)$ as $e = 2$

$K = K1(b/a)$ as $e = 1$

$K = K2(b/a)$ as $e = 0$.

(b) The combination of Case (A) and Case (F)

Residual stress distribution for this combination is shown in Figure 23. Based on the same force, σ_{cb}, we also get $\sigma_{max} = 2(1-e)\sigma_c$, but it is due to case (F).

$$\therefore \sigma = \begin{cases} e\sigma_c + 2(1-e)\sigma_c(zx/b) & 0 \leq x \leq b/2 \\ e\sigma_c + 2(1-e)\sigma_c(2-2x/b) & b/2 \leq x \leq b \end{cases} .$$

By equation (3) and the method of superposition, the stress-intensity factor equation is given as

$$\therefore K = eK1(b/a) + (1-e)K6(b/a) \qquad (11)$$

$K = K6(b/a)$ as $e = 0$

$K = K1(b/a)$ as $e = 1$

3.3 The Crack-Tip Problem

Nine basic stress patterns have been identified as possible distributions of residual stress along the crack line. However, in most engineering situations, the average value of the residual stresses or a uniform residual stress distribution is used to calculate the K-value. Thus, it is appropriate to examine the difference between the uniform residual stress pattern and the other eight residual stress patterns. These differences are expressed in percentage

$$\frac{K-K1}{K1} = \frac{F-F1(b/a)}{F1(b/a)} \times 100\% \qquad (12)$$

where K is K2, K3, K4, K5, K6, K7, K8 or K9 and F is F2, F3, F4, F5, F6, F7, F8 or F9.

These results are tabulated in Table 2. Here there is no error greater than 5% except for cases K3 and K5 at b/a equals 0.8. It is reasonable based on this to use uniform residual stresses in calculating K-values since this introduces no appreciable errors. Moreover, the residual stress distributions which lead to K3 and K5 are much steeper than the others. This is not regarded as happening very often. Thus, it will not be given further consideration here. Now the largest error at b/a = 0.9 is 7.637% for K2 and K4. Prior to this, the uniform stress pattern should be regarded as valid. After b/a = 0.9 much larger errors will be induced. Thus, the so-called "near-crack-tip region" here is defined as from b/a = 0.9 to b/a = 1.0.

At this point, the residual stresses near the crack tip have been proven more influential on the K-value than those away from the crack tip. Thus, superposing other stress patterns in addition to a uniform stress pattern in the near-crack-tip region is required. Three cases are considered with the uniform stress pattern, an isosceles-triangular stress pattern, a parabolic stress pattern, and a uniform stress pattern. Their geometries are shown in Figure 24.

(a) For uniform stress, the stress-intensity factor for b/a from 0.9 to 1.0 with $\sigma_{max}=\sigma_c$ is

$$\Delta K = K1(1)-K1(0.9) = \frac{\sigma_c\sqrt{\pi a}}{\pi(1)^2} F1(1) - \frac{\sigma_c\sqrt{\pi a}}{\pi(0.9)^2} F1(0.9)$$

$$= \frac{\sigma_c\sqrt{\pi a}}{\pi} [F1(1) - F1(0.9)/0.81]$$

in which σ_c can be replaced by $\gamma\sigma_c$ and γ is the ratio of b_{max} by σ_c.

By adding ΔK to the uniform stress pattern which is specified as b/a from 0 to 1,

$$K = K1(1)+\Delta K = \frac{b_c\sqrt{\pi a}}{\pi(1)^2} F_1(1) + \frac{\gamma\sigma_c\sqrt{\pi a}}{\pi} [F1(1) - \frac{F1(0.9)}{0.81}]$$

$$= \frac{\sigma_c\sqrt{\pi a}}{\pi} [(\gamma+1)F1(1) - \frac{\gamma F1(0.9)}{0.81}]$$

$$= \frac{\sigma_c\sqrt{\pi a}}{\pi} F_I \qquad \Bigg\} \qquad (13)$$

where $F_I = (\gamma+1)F1(1) - \frac{\gamma F1(0.9)}{0.81}$

$$\frac{K-K1(1)}{K1(1)} = \frac{\Delta K}{K1(1)} = \frac{F_I-F1(1)}{F1(1)} \times 100\% \qquad (14)$$

Numerical values of F_I and results in equation (14) are tabulated in Table 3.

(b) For parabolic stress pattern,

$$\sigma = \gamma\sigma_c[1-(\frac{x-0.95a}{0.05a})^2]$$

$$= \gamma\sigma_c[1-400(\frac{x}{a} - 0.95)^2] \qquad 0.9a \leq x \leq a$$

Similar to case (a), this yields

$$K = \frac{\sigma_c\sqrt{\pi a}}{\pi} F_{II} \tag{15}$$

$$\frac{K-K1(1)}{K1(1)} = \frac{\Delta K}{K1(1)} = \frac{F_{II}-F1(1)}{F1(1)} \times 100\% \tag{16}$$

Numerical values of F_{II} and results in equation (16) are tabulated in Table 4.

(c) For isosceles-triangular stress pattern,

$$\sigma = \begin{cases} 20\gamma\sigma_c(x/a-0.9) & 0.9a \leq x \leq 0.95a \\ 20\gamma\sigma_c(1-x/a) & 0.95a \leq x \leq a \end{cases}$$

$$\therefore \Delta K = \int_{0.9a}^{0.95a} \frac{2[20\gamma\sigma_c(x/a-0.9)]dx}{\sqrt{\pi a}} \frac{F(x/a)}{\sqrt{1-(x/a)^2}}$$

$$+ \int_{0.95a}^{a} \frac{2[20\gamma\sigma_c(1-x/a)]dx}{\sqrt{\pi a}} \frac{F(x/a)}{\sqrt{1-(x/a)^2}}$$

Again, similar to case (a), this yields

$$K = \frac{\sigma_c \sqrt{\pi a}}{\pi} F_{III} \tag{17}$$

$$\frac{K-K1(1)}{K1(1)} = \frac{\Delta K}{K1(1)} = \frac{F_{III}-F1(1)}{F1(1)} \times 100\% \tag{18}$$

Numerical values of F_{III} and results in equation (18) are tabulated in Table 5.

4. DISCUSSION AND CONCLUSION

This paper discusses the possible effect due to various residual stresses on fatigue and fracture behavior of structural members. The variability of residual stresses definitely affects the value of the maximum stress-intensity factor, K_{max}, corresponding to σ_{max}. As such this must be considered when a fracture failure will happen.

As for the fatigue-crack-propagation behavior, the crack growth rate generally can be represented by

$$\frac{da}{dN} = C(\Delta K)^n \qquad 2 < n < 4 \tag{19}$$

where a = crack length

N = number of cycles

ΔK = stress-intensity factor fluctuation

c and n are constants.

Note that existing fatigue cracks will not propagate when ΔK is below the critical value ΔK_{th} - the fatigue-crack - initiation threshold. ΔK_{th} has been shown in many experiments to depend on the magnitude of stress ratio, $R = \sigma_{min}/\sigma_{max} = K_{min}/K_{max}$. Conservative estimates of ΔK_{th} for martensitic steels, ferrite-pearlite steels, and austenitic steels subjected to various R values larger than +0.1 can be predicted from[9]

$$\Delta K_{th} = 6.4(1-0.58R) \qquad (20)$$

where ΔK_{th} is in ksi$\sqrt{in}$ and is equal to 5.5 ksi$\sqrt{in}$(6 MN/m$^{-3/2}$) as $R < 0.1$.

Since the variability of residual stresses affects changes in R value and doesn't change the magnitude of ΔK, then the effect of residual stress on fatigue-crack-initiation and propagation behavior can be studied through the R-ratio.

Available experimental data on A514 Grade B steel show no systematic change in fatigue-crack-growth rate with changes in R value from 0 to 0.82[10], that is, this change in R value has negligible effects on the rate of crack propagation in the region where ΔK is greater than ΔK_{th}. Other data on fatigue-crack growth in a 140 ksi (965 MN/m^2) yield strength martensitic steel[11] show a systematic increase in growth rate with increase in R value from 0 to 0.75 and with decrease

in R from 0 to -2, nevertheless the maximum increase in fatigue-crack-growth rate as function of variation of R from -2 to 0.75 is less than a factor of 2. Because ΔK is the primary driving force for crack-propagation, together with preceding discussions, even high stress ratios - high residual stresses - have negligible effect on the fatigue-crack-growth rate behavior at ΔK greater than ΔK_{th}.

On the otherhand, high residual stresses which also mean high stress ratio, will decrease ΔK_{th} from equation (20). Thus, fatigue cracks in regions of tensile-residual stresses are initiated at lower ΔK levels.

In order to predict accurately the value of K_c and ΔK_{th} for various materials and structures, the contribution near the crack tip from residual stress becomes very significant. Thus, it is suggested that the several residual stress patterns examined near the crack-tip can be combined by superposition to accurately predict K values.

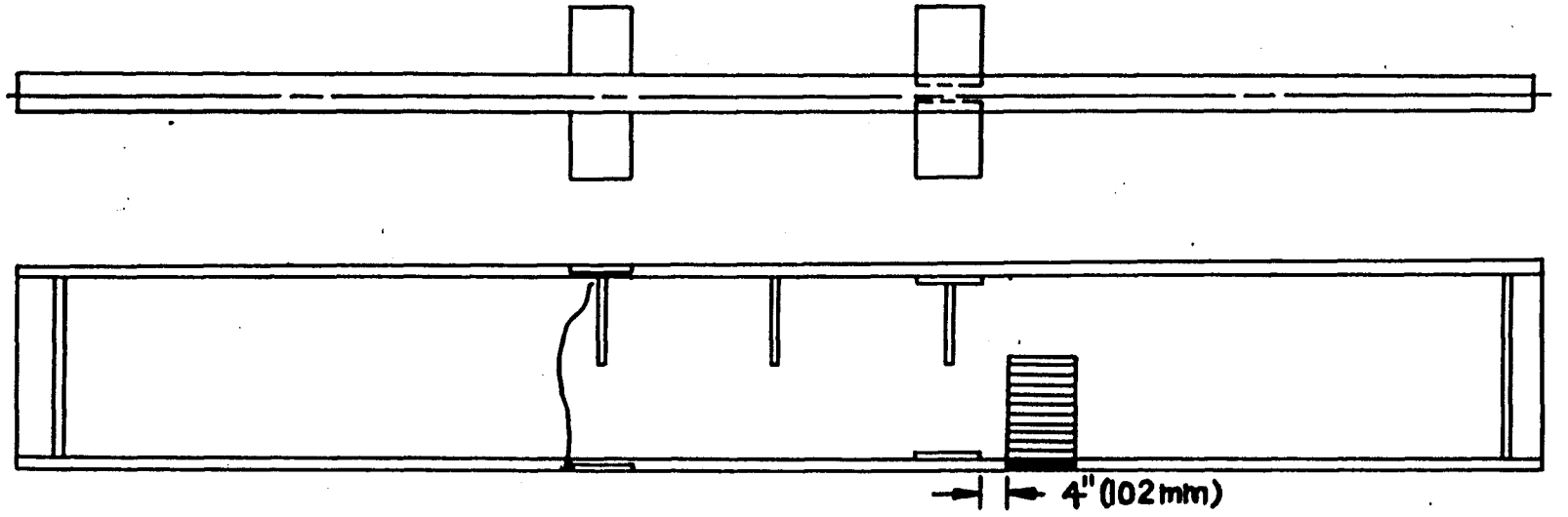

Fig. 1. Sliced Region of Welded Beam, Steel A36

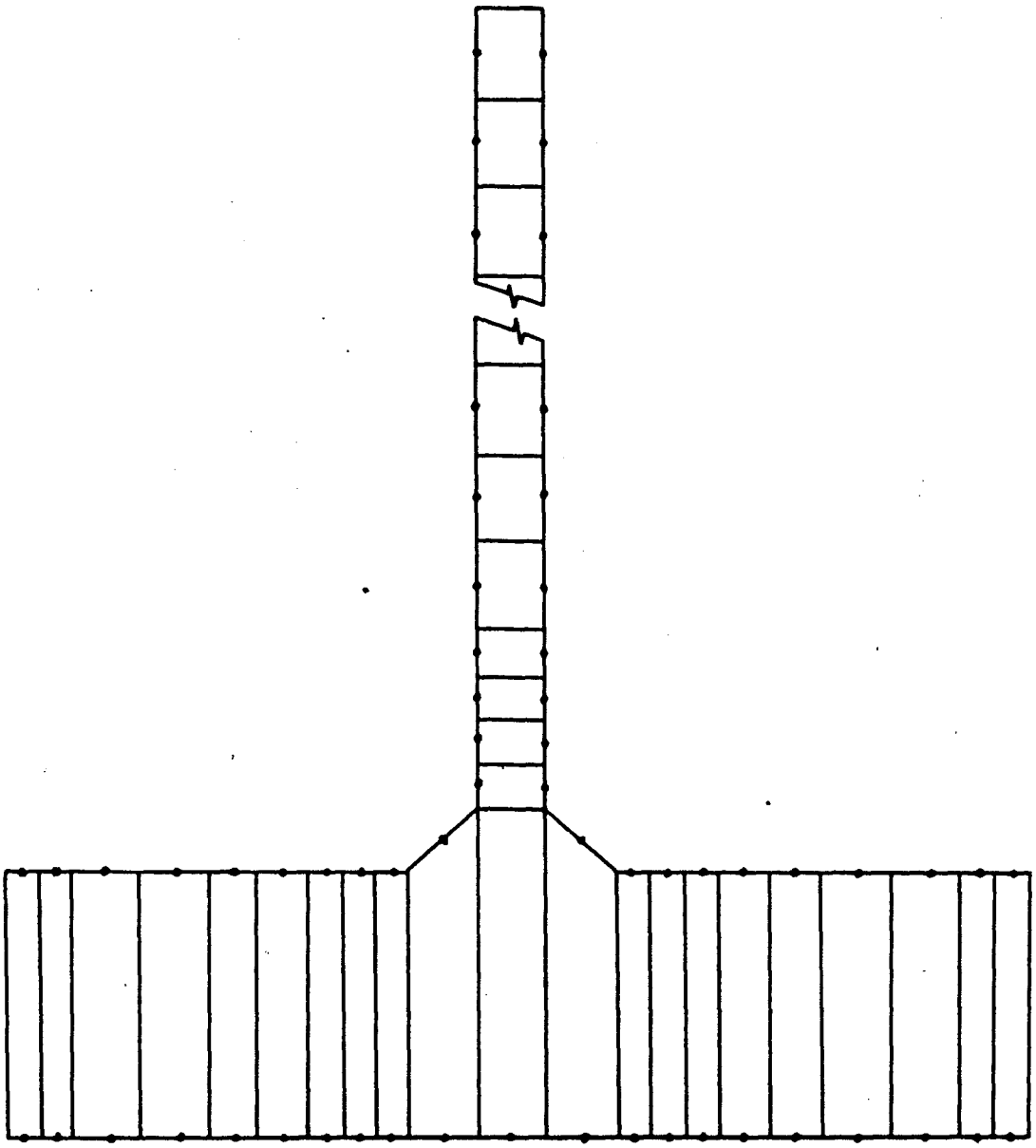

Fig. 2. Cross-Section of Sliced Welded Beam

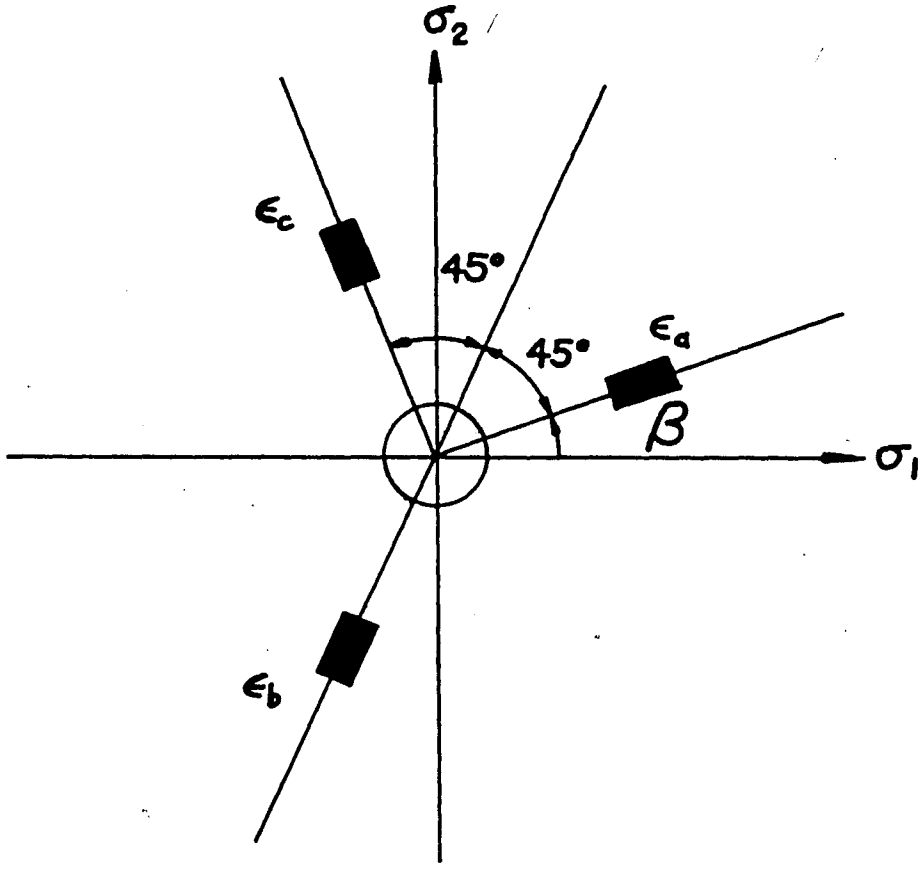

Fig. 3. Strain Rosette Stress Field Orientation

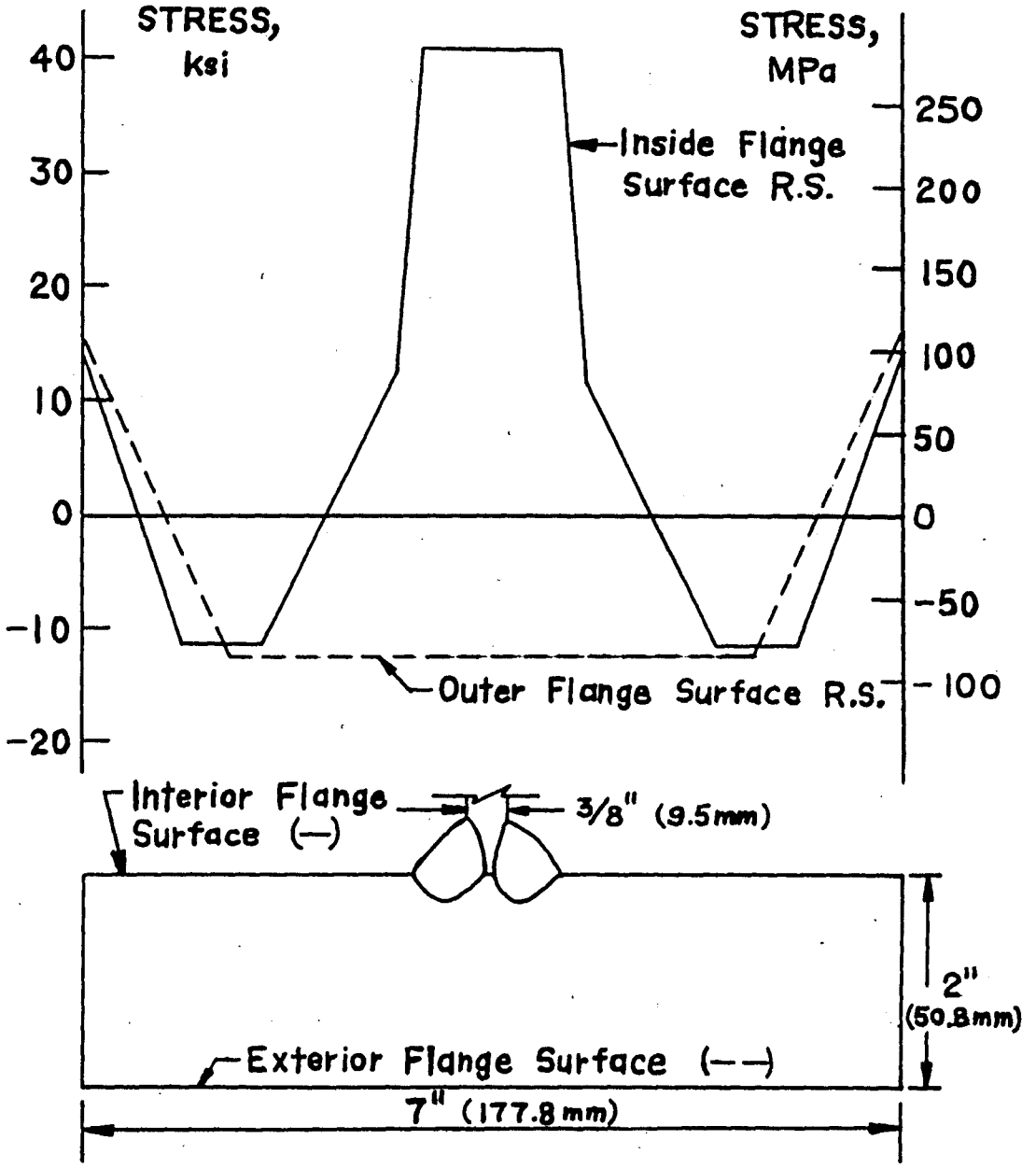

Fig. 4. Measured Residual Stress Distribution for A36 Flange

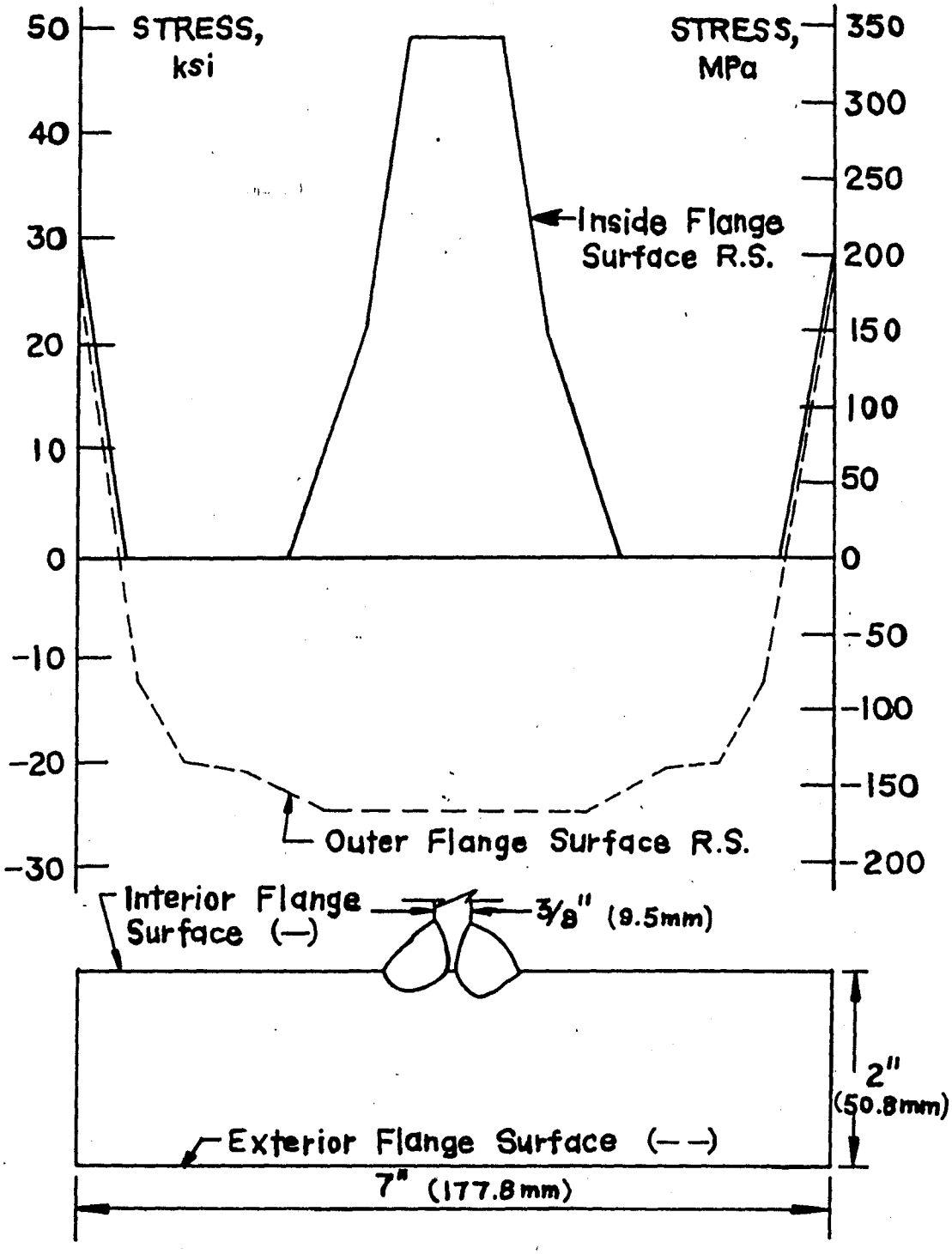

Fig. 5. Measured Residual Stress Distribution for A588 Flange

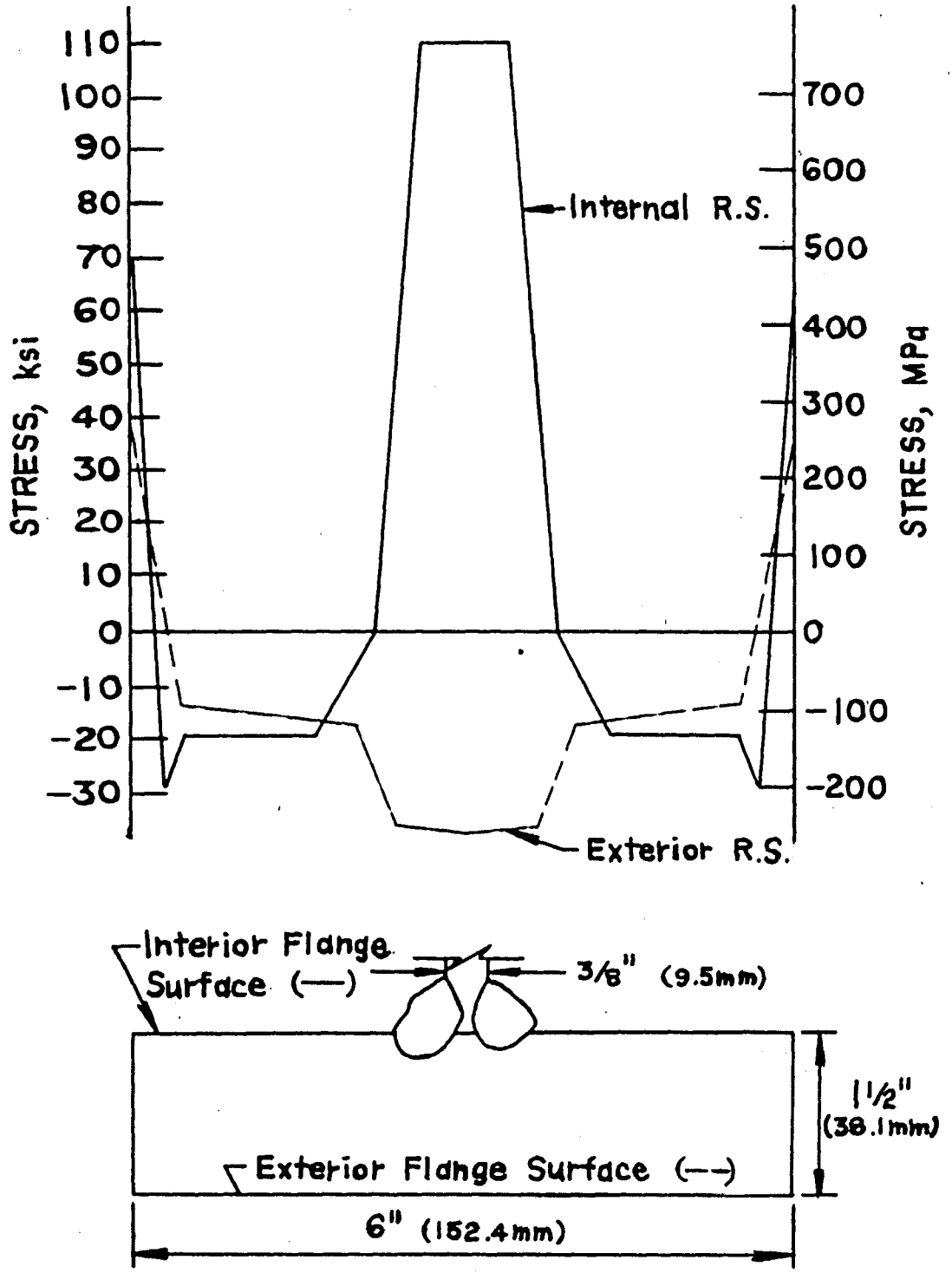

Fig. 6. Measured Residual Stress Distribution for A514 Flange

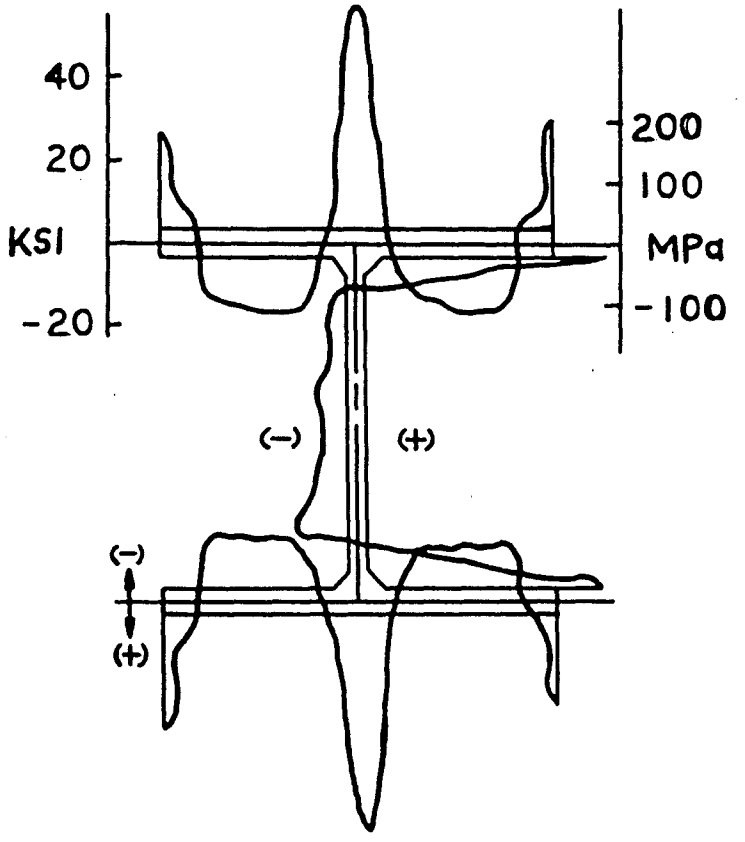

Fig. 7. Averaged Residual Stress for 12H79 Flange

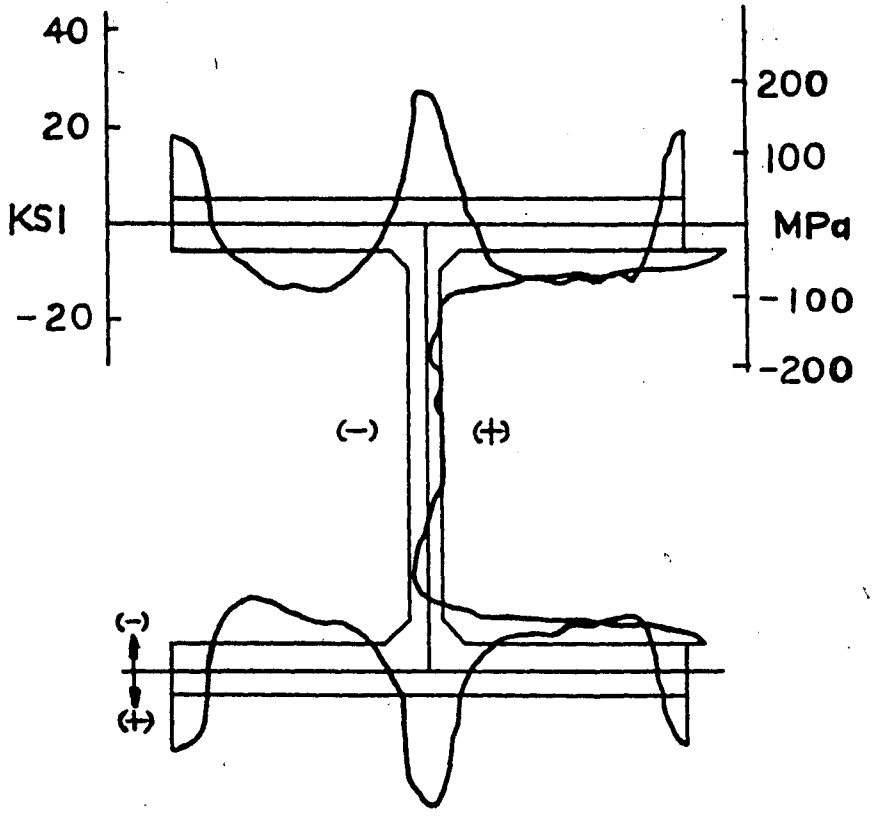

Fig. 8. Averaged Residual Stress for 14H202 Flange

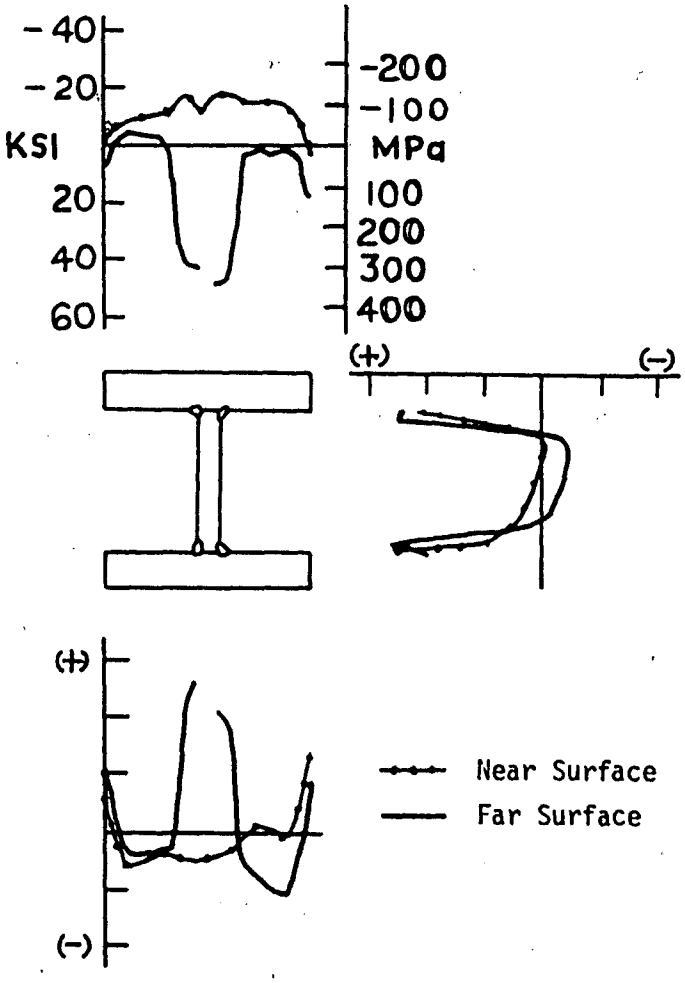

Fig. 9. Residual Stresses in a Welded Shape 15H290 -Flamecut Plates, A36 Steel, 1/2 in. Fillet Welds

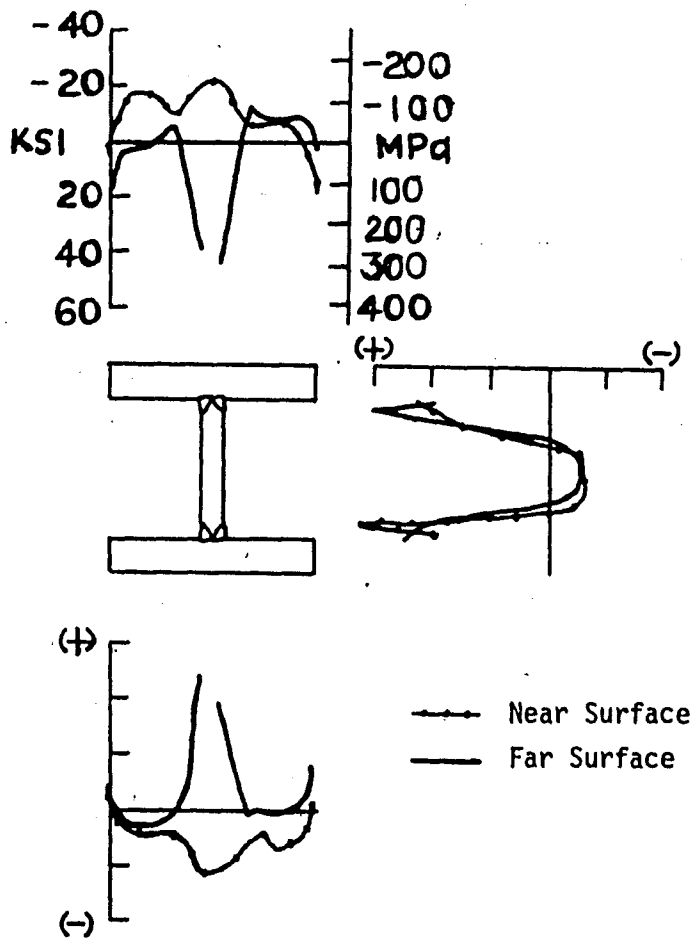

Fig. 10. Residual Stresses in a Welded Shape 15H290 -Flamecut Plates, A36 Steel, 11/16 in. Groove Welds

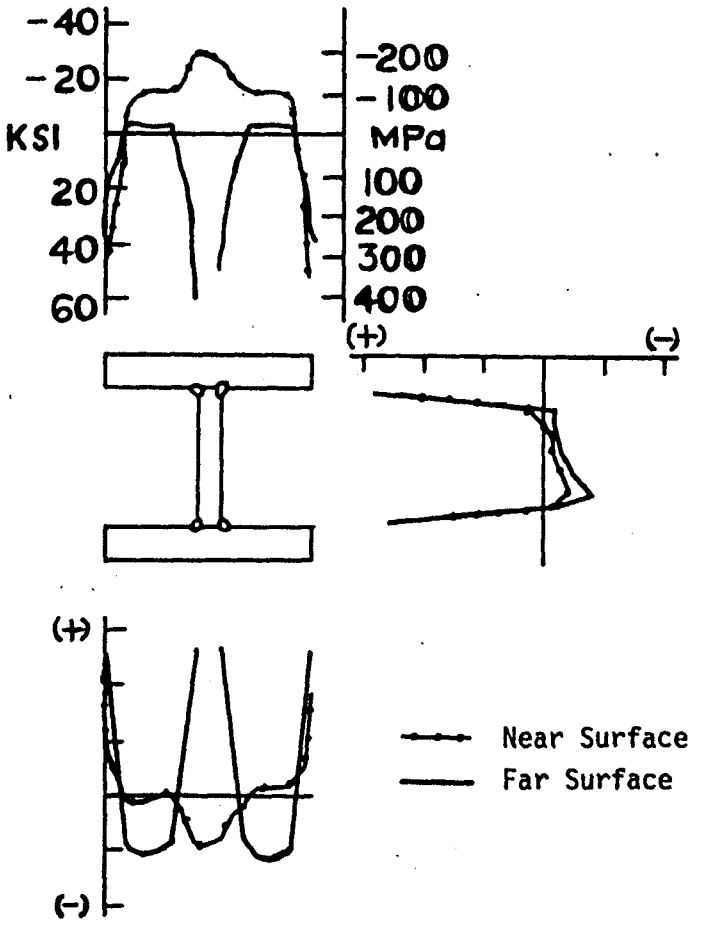

Fig. 11. Residual Stresses in a Welded Shape 15H290 -Flamecut Plates, A441 Steel, 1/2 in. Fillet Welds

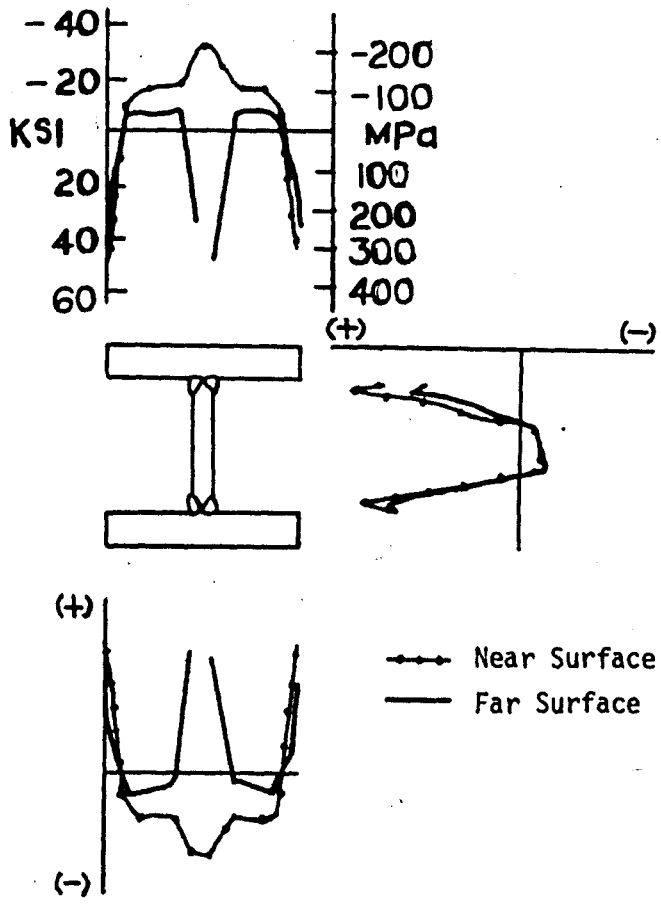

Fig. 12. Residual Stresses in a Welded Shape 15H290 -Flamecut Plates, A441 Steel, 11/16 in. Groove Welds

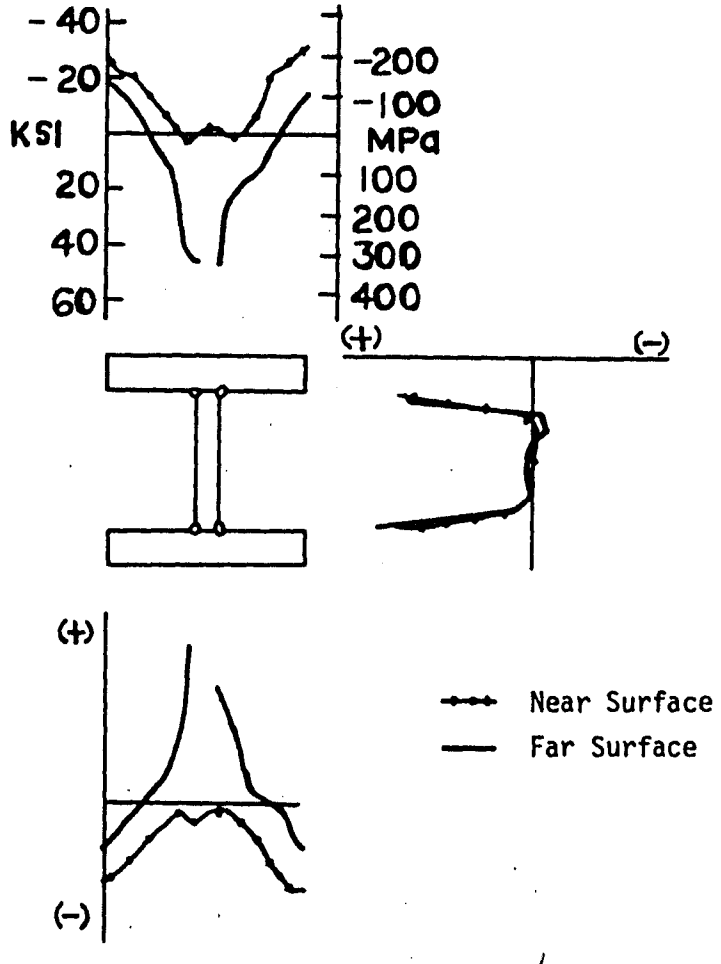

Fig. 13. Residual Stresses in a Welded Shape 15H290 -Universal-mill Plates, A36 Steel, 1/2 in. Fillet Welds

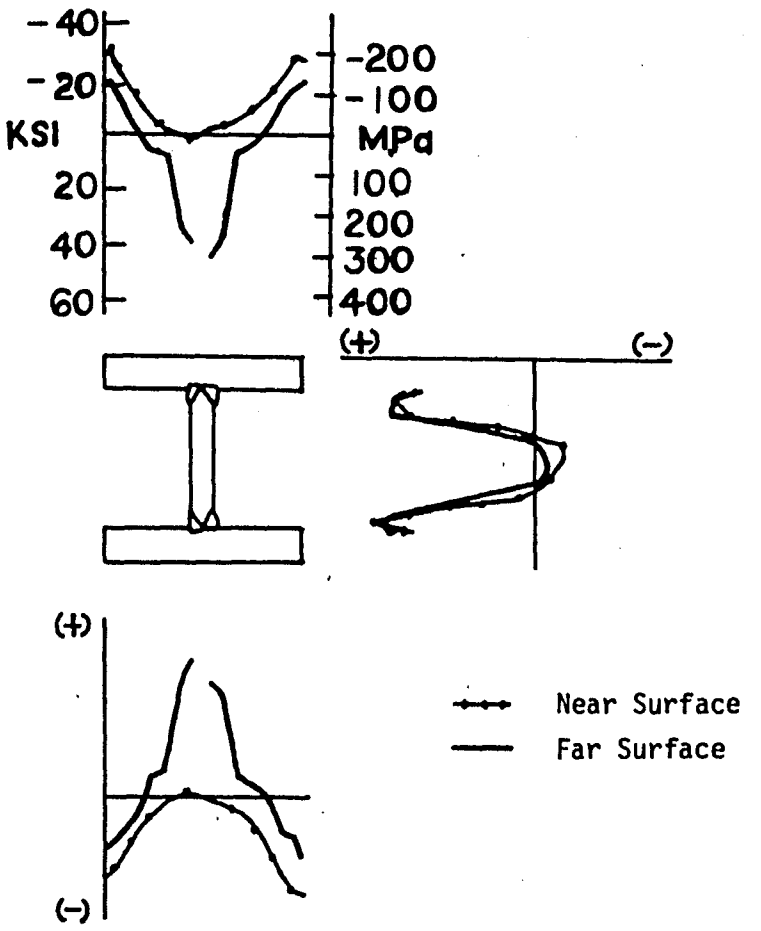

Fig. 14. Residual Stresses in a Welded Shape 15H290 -Universal-mill Plates, A36 Steel, 11/16 in. Groove Welds

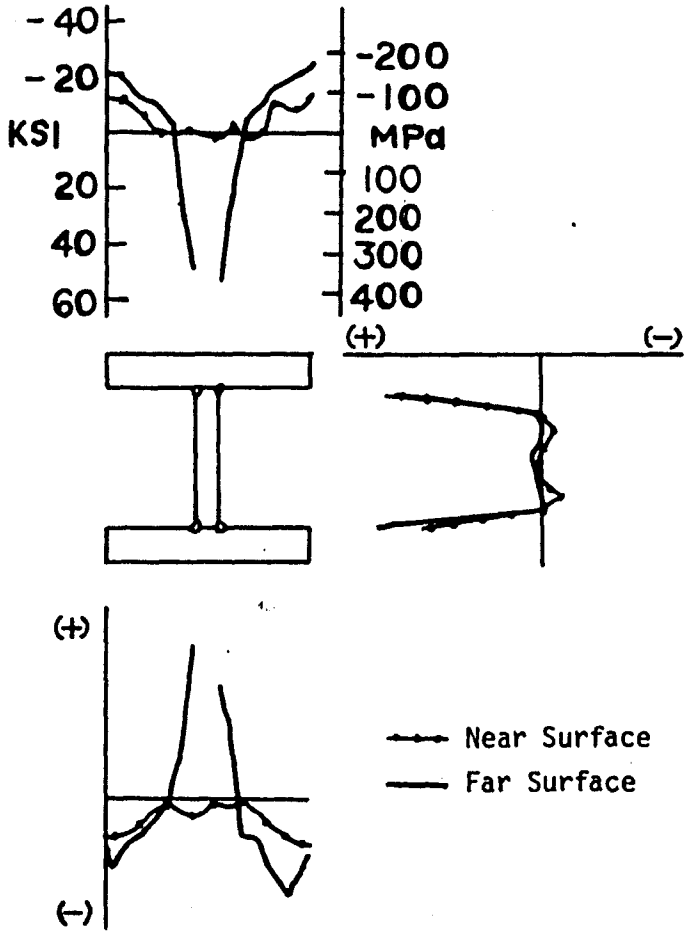

Fig. 15. Residual Stresses in a Welded Shape 15H290 -Universal-mill Plates, A441 Steel, 1/2 in. Fillet Welds

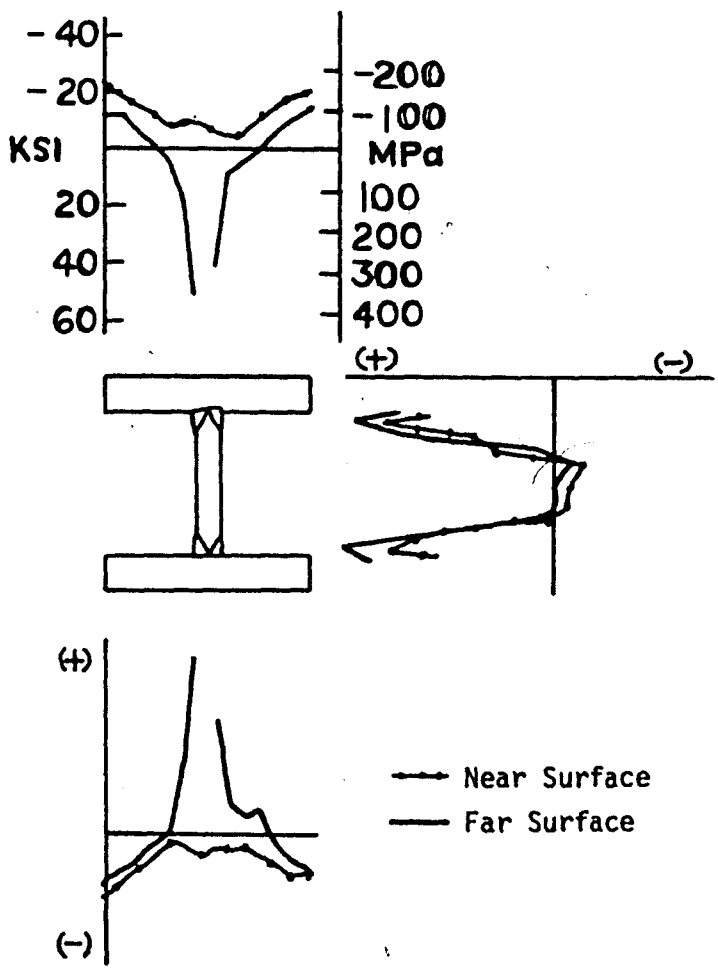

Fig. 16. Residual Stresses in a Welded Shape 15H290 -Universal-mill Plates, A441 Steel, 11/16 in. Groove Welds

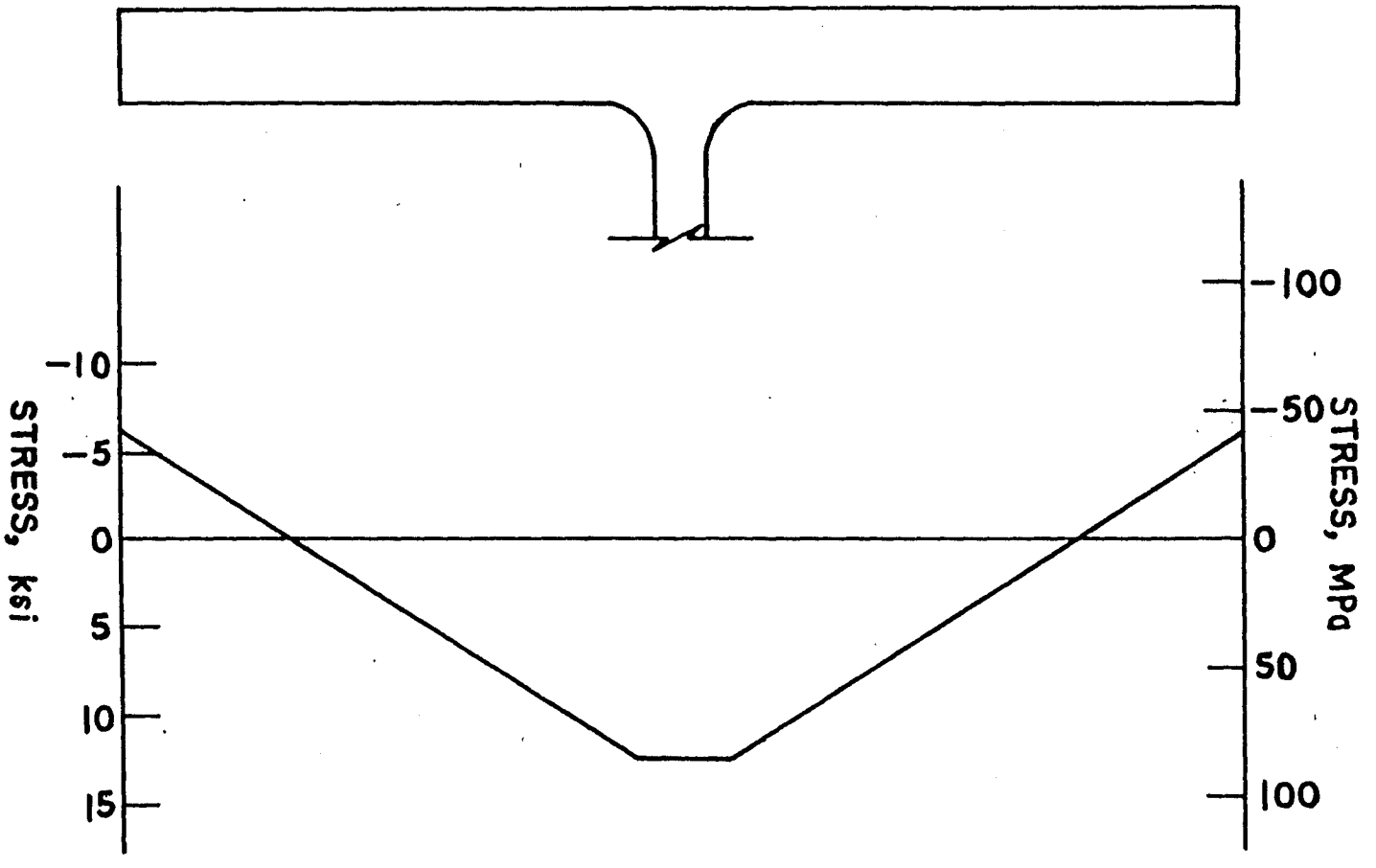

Fig. 17. Measured Residual Stress Distribution for A36, W36x2360, Flange

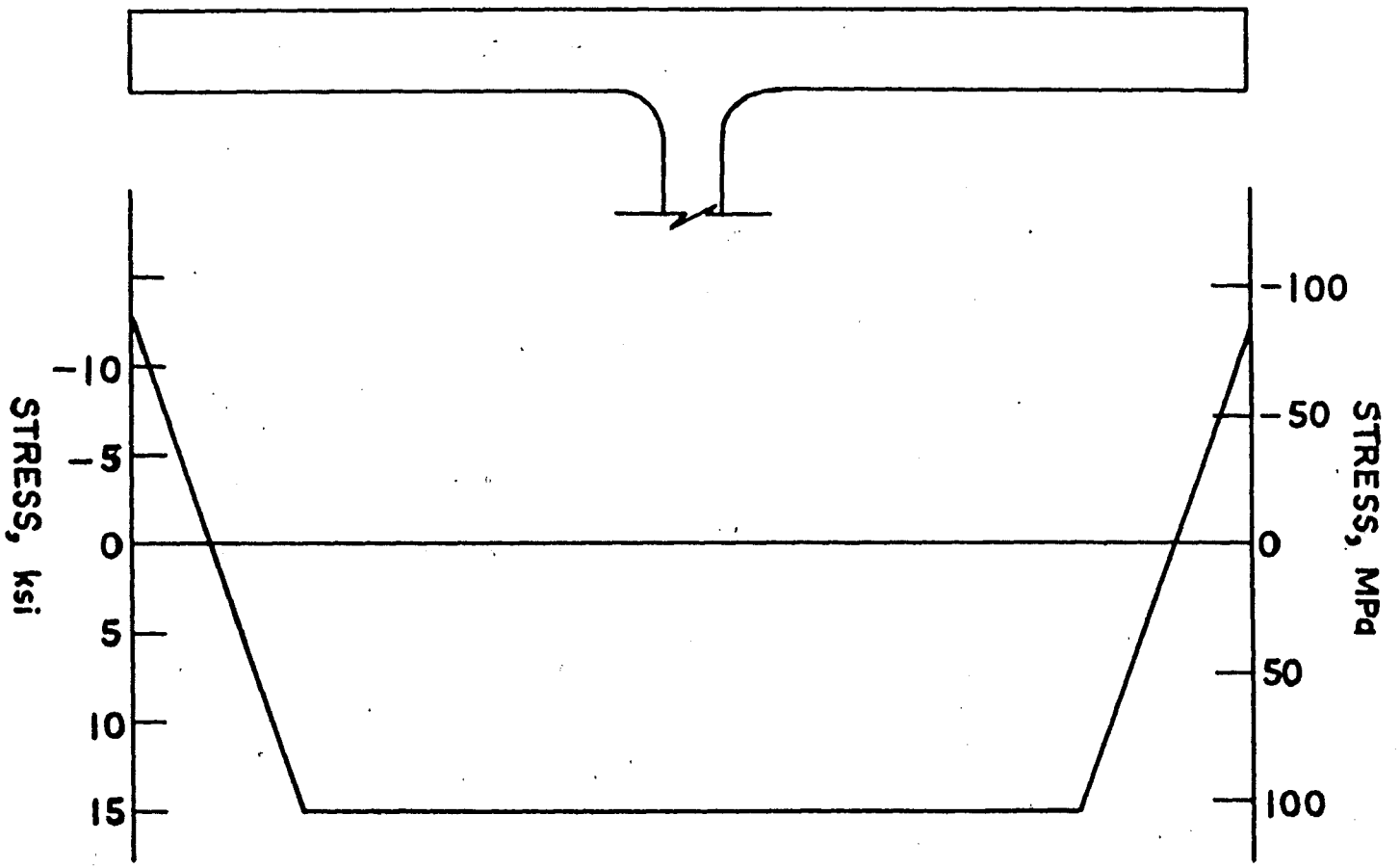

Fig. 18. Measured Residual Stress Distribution for A588, W36x230, Flange

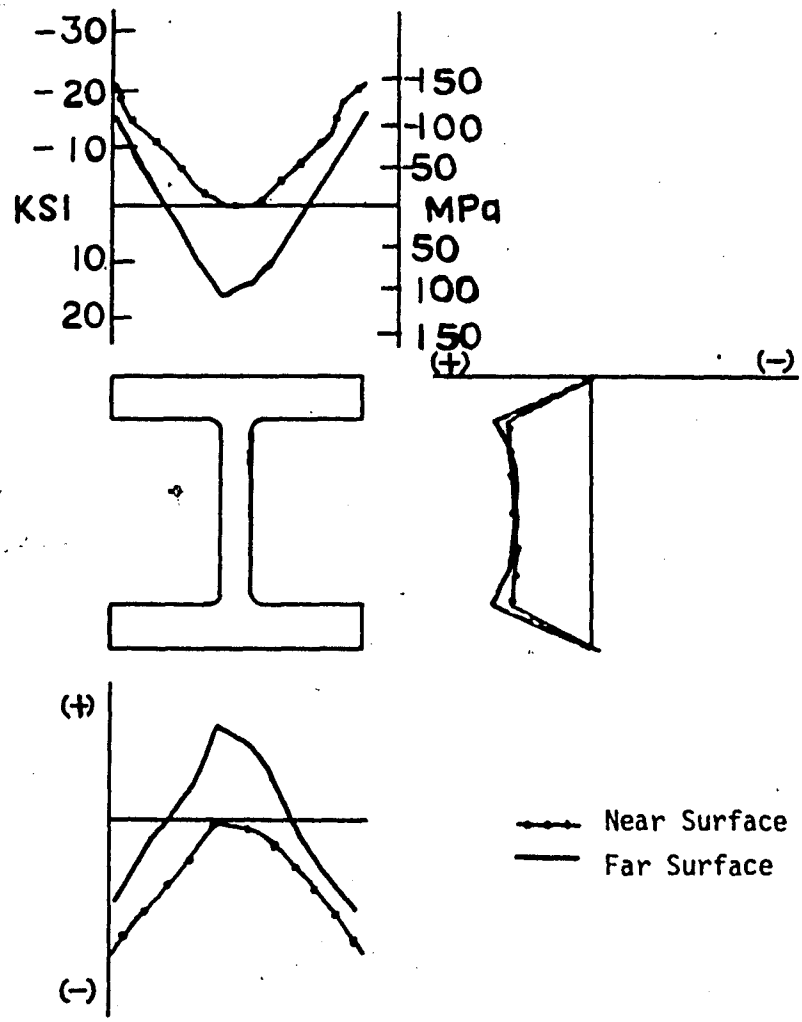

Fig. 19. Residual Stresses in a Hot-rolled Shape 14WF 426, A7 Steel

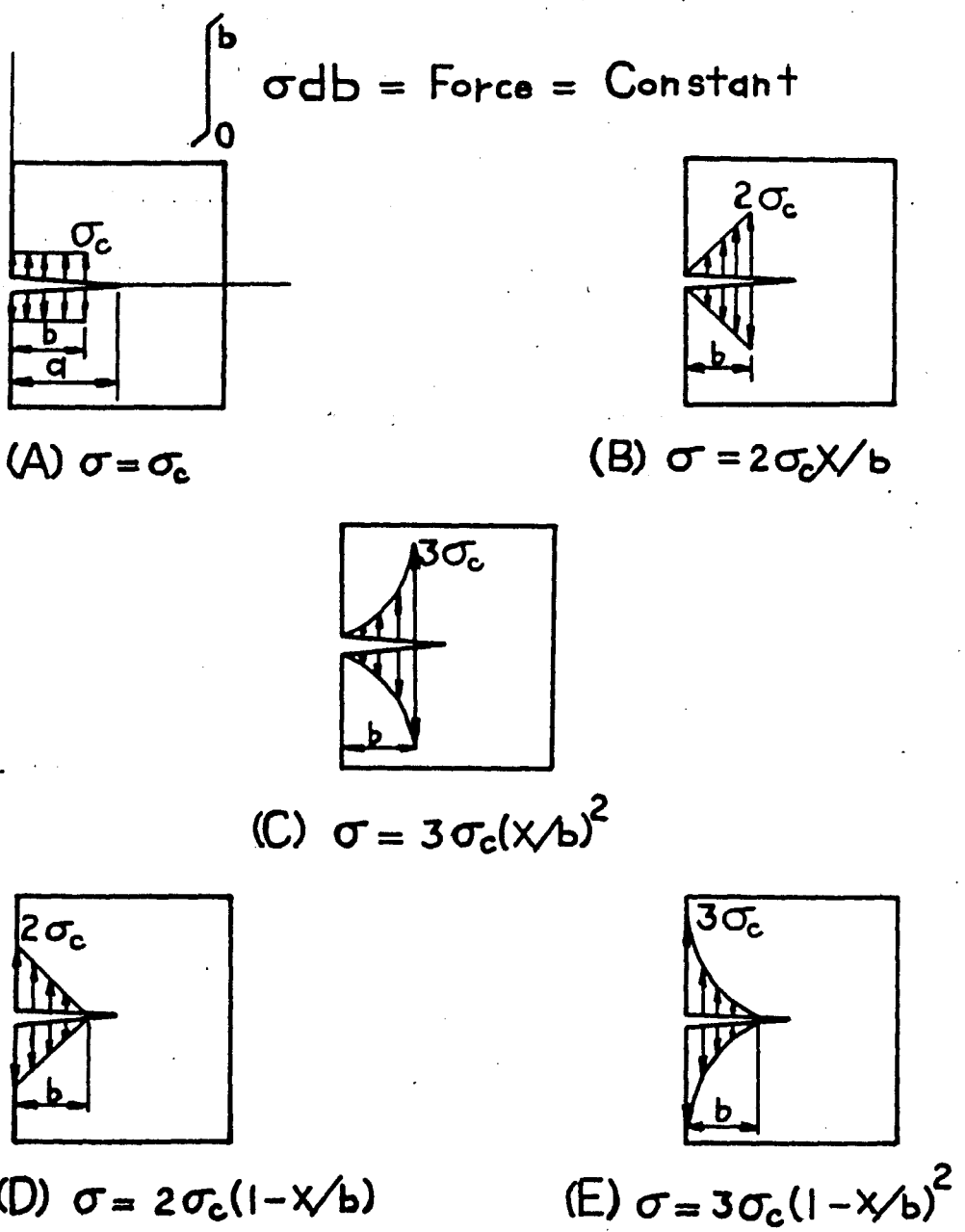

Fig. 20. Nine Different Distributions of Residual Stress along the Whole Single-edge Crack

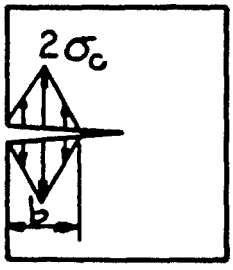

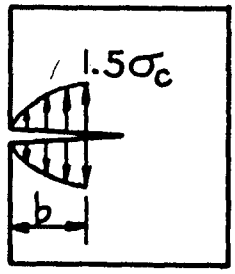

$$(F)\ \sigma = \begin{cases} 2\sigma_c(2X/b) & 0 \le X \le b/2 \\ 2\sigma_c(2-2X/b) & b/2 \le X \le b \end{cases}$$

$$(G)\ \sigma = 1.5\sigma_c\left[1-(1-X/b)^2\right]$$

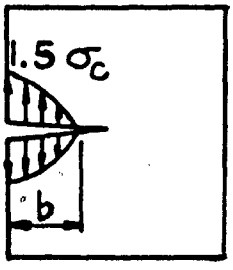

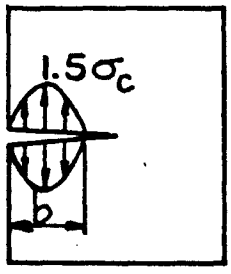

$$(H)\ \sigma = 1.5\sigma_c\left[1-(X/b)^2\right]$$

$$(I)\ \sigma = 1.5\sigma_c\left[1-\left(\frac{2X-b}{b}\right)^2\right]$$

Fig. 20. (Continued)

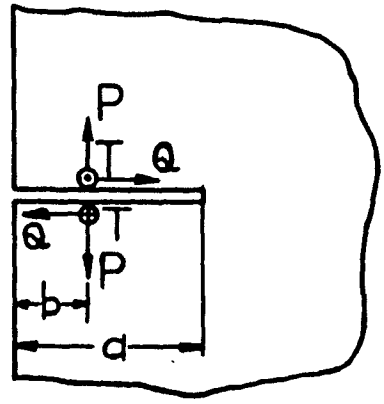

$$\begin{Bmatrix} K_I \\ K_{II} \\ K_{III} \end{Bmatrix} = \frac{2}{\sqrt{\pi a}} \begin{Bmatrix} P \\ Q \\ T \end{Bmatrix} \frac{1}{\sqrt{1-(b/a)^2}} \begin{Bmatrix} F(b/a) \\ F(b/a) \\ 1 \end{Bmatrix}$$

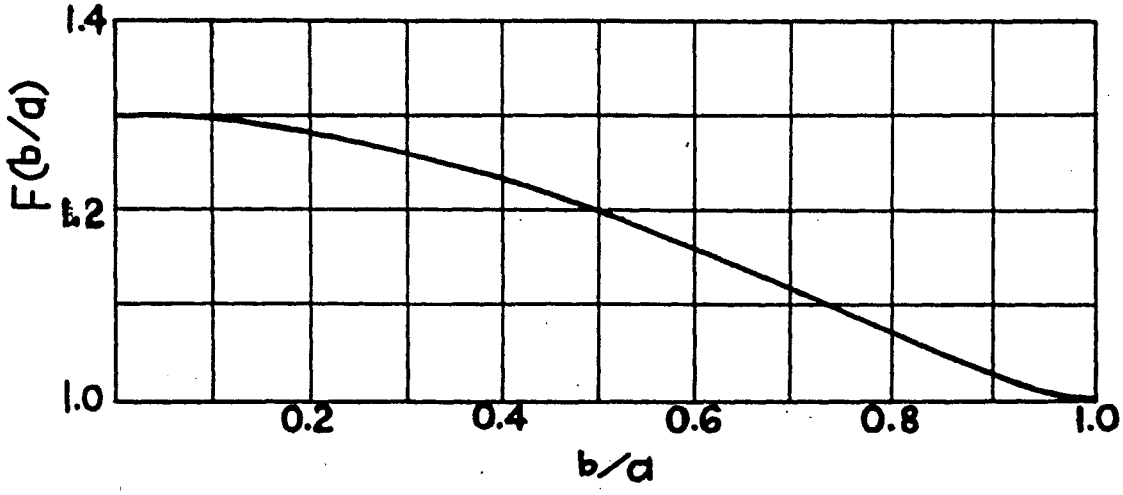

Fig. 21. F(b/a) vs. b/a in Equation (3)

$$K_1 = \frac{2\sigma_b}{\pi}\sqrt{\pi a}\,\sin^{-1}(b/a)\,FA(b/a)$$

$$K_2 = \frac{4\sigma_b}{\pi}\,\frac{\sqrt{\pi a}}{b/a}\,FB(b/a)$$

$$K_3 = \frac{6\sigma_b}{\pi}\,\frac{\sqrt{\pi a}}{(b/a)^2}\,FC(b/a)$$

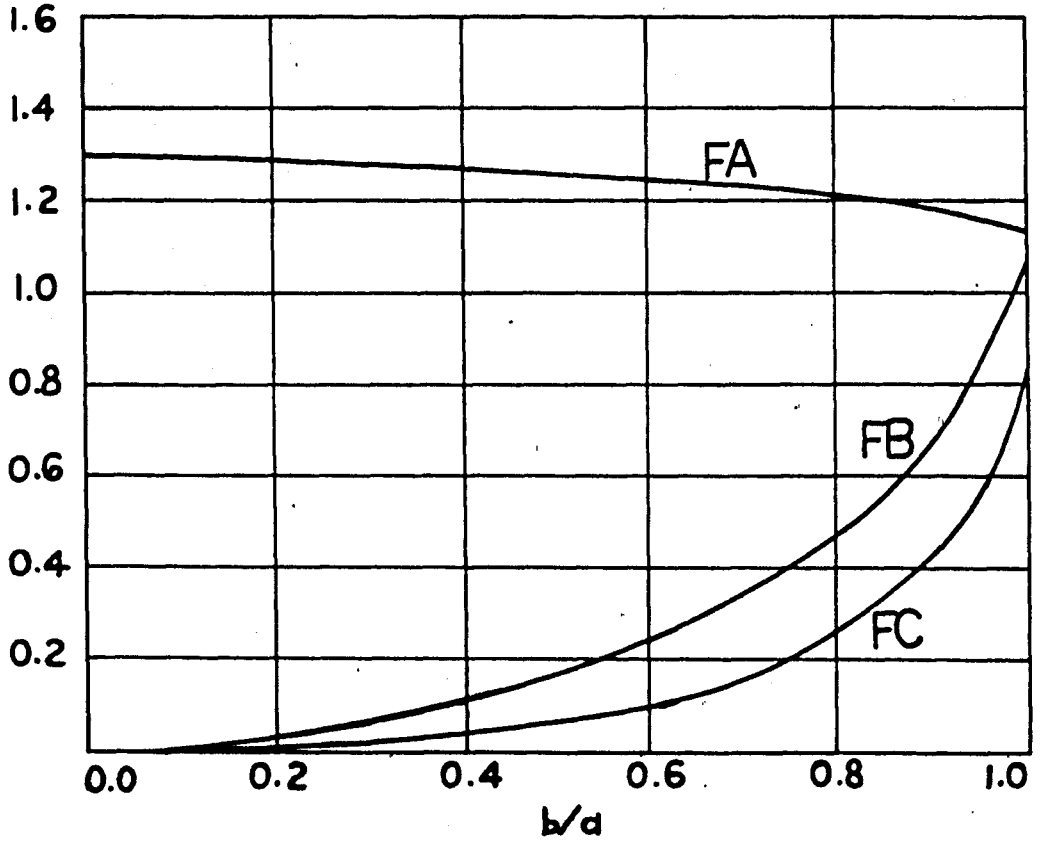

Fig. 22. The Plot of FA, FB and FC vs. b/a in Eq. (4)

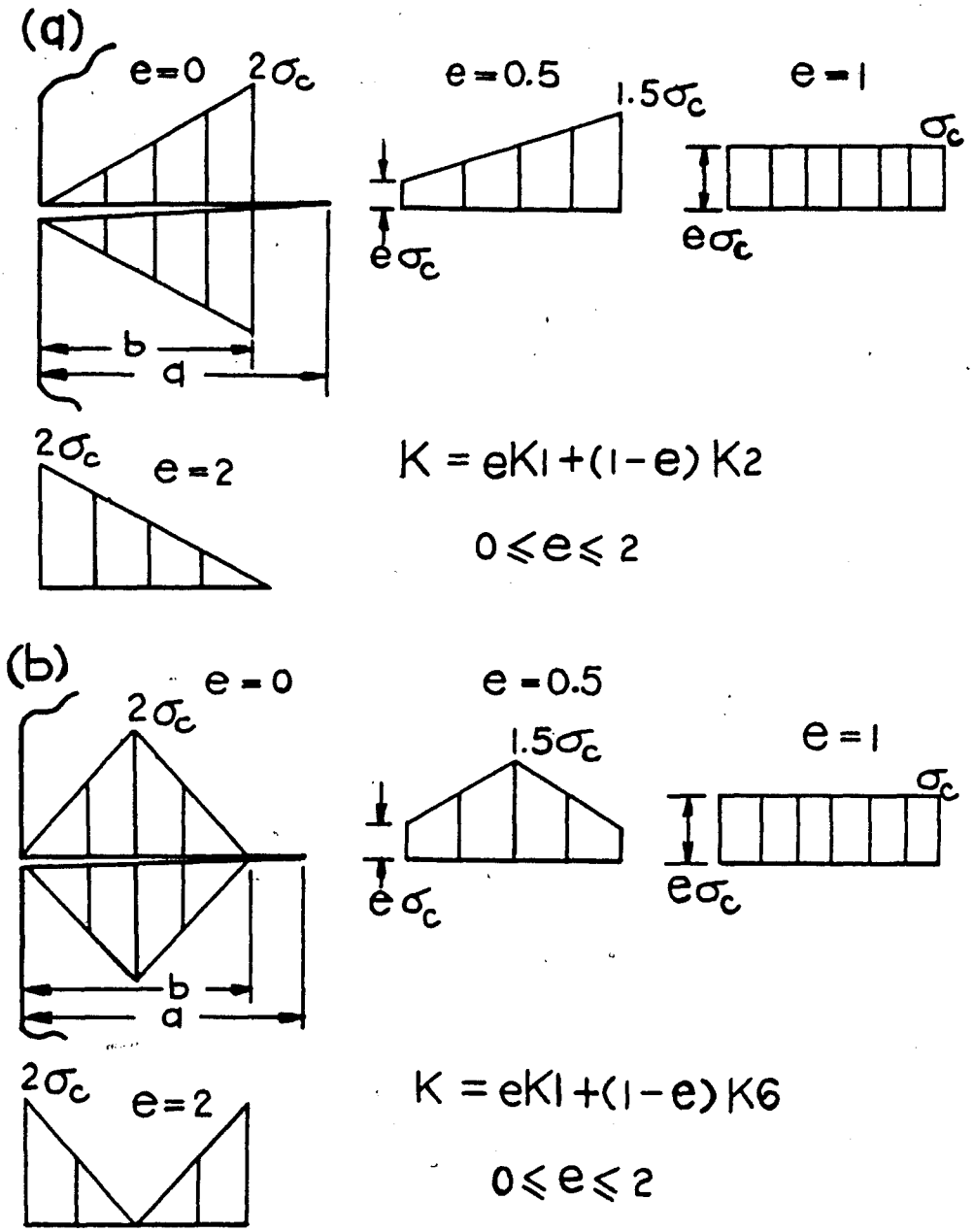

Fig. 23. Two Families of Residual Stress Patterns in Equations (10) and (11)

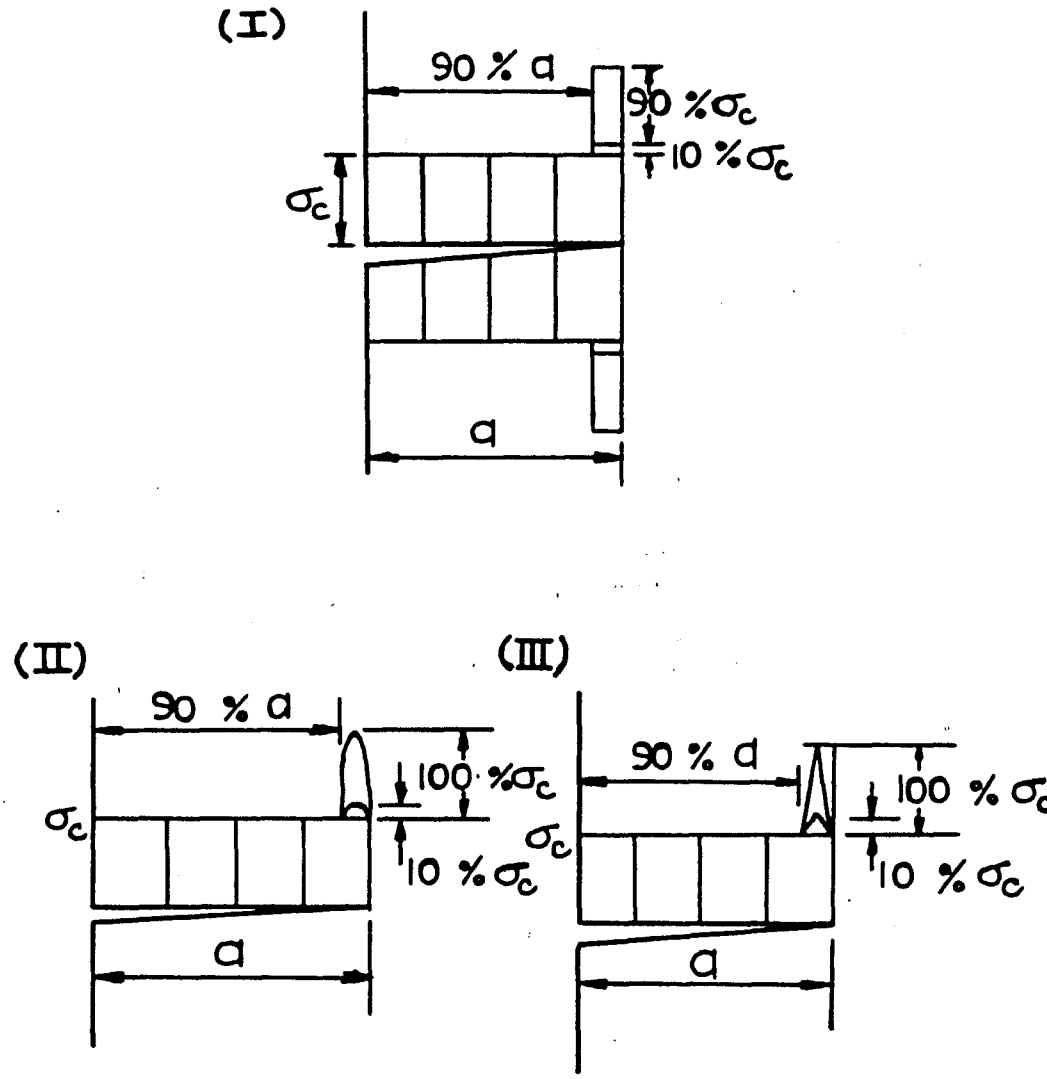

Fig. 24. Superposed Models Near the Crack Tip in Equations (13) to (18)

b/a \ F	F1(b/a)	F2(b/a)	F3(b/a)	F4(b/a)	F5(b/a)	F6(b/a)	F7(b/a)	F8(b/a)	F9(b/a)
0.0	0.	0.	0.	0.	0.	0.	0.	0.	0.
0.1	.0026	.0026	.0026	.0026	.0026	.0026	.0026	.0026	.0026
0.2	.0208	.0208	.0208	.0208	.0208	.0208	.0208	.0208	.0208
0.3	.0702	.0706	.0707	.0702	.0701	.0703	.0705	.0202	.0703
0.4	.1677	.1686	.1692	.1667	.1664	.1674	.1683	.1669	.1674
0.5	.3299	.3331	.3351	.3267	.3256	.3289	.3321	.3273	.3291
0.6	.5767	.5862	.5924	.5672	.5640	.5731	.5831	.5689	.5737
0.7	.9320	.9571	.9741	.9068	.8986	.9212	.9486	.9109	.9232
0.8	1.4300	1.4934	1.5377	1.3666	1.3475	1.3994	1.4713	1.3762	1.4049
0.9	2.1377	2.3009	2.4206	1.9744	1.9308	2.0468	2.2411	1.9963	2.0617
1.0	3.5502	4.3171	4.9745	2.7833	2.6737	2.9527	3.9885	2.8331	3.0024

Table 1. The Tabulated Values of F in Equations (4) to (9)

b/a \ F	F1(b/a)	F2(b/a)	F3(b/a)	F4(b/a)	F5(b/a)	F6(b/a)	F7(b/a)	F8(b/a)	F9(b/a)
0.80	1.4300	1.4934	1.5377	1.3666	1.3475	1.3994	1.4713	1.3762	1.4049
0.82	1.5515	1.6274	1.6815	1.4753	1.4527	1.5138	1.6010	1.4866	1.5204
0.84	1.6819	1.7737	1.8389	1.5901	1.5635	1.6352	1.7411	1.6034	1.6433
0.86	1.8221	1.9328	2.0122	1.7113	1.6799	1.7641	1.8931	1.7270	1.7740
0.88	1.9734	2.1075	2.2047	1.8393	1.8023	1.9011	2.0589	1.8578	1.9132
0.90	2.1377	2.3009	2.4206	1.9744	1.9308	2.0468	2.2411	1.9963	2.0617
0.92	2.3177	2.5138	2.6672	2.1172	2.0657	2.2021	2.4438	2.1430	2.2204
0.94	2.5180	2.7678	2.9563	2.2683	2.2071	2.3679	2.6735	2.2989	2.3907
0.96	2.7467	3.0651	3.3104	2.4284	2.3553	2.5459	2.9424	2.4649	2.5745
0.98	3.0241	3.4493	3.7862	2.5989	2.5107	2.7387	3.2808	2.6430	2.7753
1.00	3.5502	4.3171	4.9745	2.7833	2.6737	2.9527	3.9885	2.8381	3.0024

Table 1. (continued) The Detailed Values of F Near the Crack-Tip

b/a \ F	F2(b/a)	F3(b/a)	F4(b/a)	F5(b/a)	F6(b/a)	F7(b/a)	F8(b/a)	F9(b/a)
0.	0.	0.	0.	0.	0.	0.	0.	0.
0.1	-0.046	-0.060	0.046	0.077	-0.021	-0.038	0.030	-0.017
0.2	0.080	0.155	-0.080	-0.086	-0.086	0.043	-0.077	-0.069
0.3	0.287	0.483	-0.287	-0.379	-0.129	0.190	-0.241	-0.103
0.4	0.558	0.913	-0.558	-0.762	-0.184	0.381	-0.456	-0.151
0.5	0.967	1.582	-0.967	-1.317	-0.322	0.659	-0.791	-0.265
0.6	1.644	2.724	-1.644	-2.206	-0.629	1.103	-1.362	-0.518
0.7	2.699	4.521	-2.699	-3.577	-1.157	1.788	-2.260	-0.944
0.8	4.433	7.528	-4.433	-5.770	-2.139	2.885	-3.764	-1.758
0.9	7.637	13.234	-7.639	-9.677	-4.252	4.839	-6.617	-3.556
1.0	21.602	40.119	-21.602	-24.688	-16.830	12.344	-20.059	-15.430

$$\frac{K-K1}{K} = \frac{F-F1(b/a)}{F1(b/a)} \times 100\%$$

Table 2. The Differences of F2,F3,F4,F5,F6,F7,F8 and F9 with F1 in Eq. (12)

b/a \ F	F2(b/a)	F3(b/a)	F4(b/a)	F5(b/a)	F6(b/a)	F7(b/a)	F8(b/a)	F9(b/a)
0.80	4.433	7.528	-4.433	-5.770	-2.139	2.885	-3.764	-1.758
0.82	4.914	8.375	-4.914	-6.369	-2.435	3.184	-4.187	-2.006
0.84	5.459	9.336	-5.459	-7.040	-2.779	3.520	-4.668	-2.296
0.86	6.079	10.438	-6.079	-7.800	-3.182	3.900	-5.219	-2.638
0.88	6.796	11.719	-6.796	-8.669	-3.665	4.334	-5.860	-3.050
0.90	7.637	13.234	-7.637	-9.677	-4.252	4.839	-6.617	-3.556
0.92	8.651	15.077	-8.651	-10.876	-4.991	5.438	-8.538	-4.201
0.94	9.919	17.407	-9.919	-12.349	-5.961	6.175	-8.704	-5.058
0.96	11.590	20.520	-11.590	-14.250	-7.310	7.125	-10.260	-6.270
0.98	14.059	25.202	-14.059	-16.976	-9.439	8.488	-12.601	-8.226
1.00	21.602	40.119	-21.602	-24.688	-16.830	12.344	-20.059	-15.430

$$\frac{K-K_1}{K_1} = \frac{F-F_1(b/a)}{F_1(b/a)} \times 100\%$$

Table 2. (continued) The Detailed Values in Equation (12) Near the Crack-Tip

$$r = \frac{\sigma_{max}}{\sigma c}$$

$$K = \frac{\sigma\sqrt{\pi a}}{\pi} F_I$$

r	F_I	$\frac{F_I - F_I(1)}{F_I(1)}$ (%)
0.1	3.6413	2.566
0.2	3.7324	5.133
0.3	3.8235	7.699
0.4	3.9147	10.270
0.5	4.0058	12.830
0.6	4.0969	15.400
0.7	4.1880	17.960
0.8	4.2791	20.530
0.9	4.3702	23.100
1.0	4.4613	25.660

Table 3. The Numerical Values in Equations (13) and (14)

$$r = \frac{\sigma_{max}}{\sigma_c}$$

$$K = \frac{\sigma\sqrt{\pi a}}{\pi} F_{II}$$

r	F_{II}	$\frac{F_{II}-F_I(1)}{F1(1)}$ (%)
0.1	3.5991	1.376
0.2	3.6479	2.752
0.3	3.6968	4.128
0.4	3.7456	5.504
0.5	3.7945	6.879
0.6	3.8433	8.225
0.7	3.8921	9.631
0.8	3.9410	11.010
0.9	3.9898	12.380
1.0	4.0387	13.760

Table 4. The Numerical Values in Equations (15) and (16)

$$r = \frac{\sigma_{max}}{\sigma_c}$$

$$K = \frac{\sigma\sqrt{\pi a}}{\pi} F_{III}$$

r	F_{III}	$\frac{F_{III}-F_I(1)}{F_I(1)}$ (%)
0.1	3.5607	0.296
0.2	3.5712	0.592
0.3	3.5817	0.888
0.4	3.5923	1.184
0.5	3.6028	1.480
0.6	3.6133	1.776
0.7	3.6238	2.072
0.8	3.6343	2.368
0.9	3.6448	2.664
1.0	3.6553	2.960

Table 5. The Numerical Values in Equations (17) and (18)

REFERENCES

1. R. Roberts, J.W. Fisher, G.R. Irwin, K.D. Boyer, H. Hausammann, G.V. Krishna, V. Morf, R.E. Slockbower, DETERMINATION OF TOLERABLE FLAW SIZES IN FULL SIZE WELDED BRIDGE DETAILS, Final Reports, Report No. FHWA-RD-77-170, Federal Highway Administration, Washington, D.C., December 1977.

2. C.P. Paris and G.C. Sih, STRESS ANALYSIS OF CRACKS, IN FRACTURE TOUGHNESS TESTING AND ITS APPLICATIONS, ASTM STP No. 381, American Society for Testing and Materials, Philadelphia, 1965.

3. H. Tada, P.C. Paris, and Ct.R. Irwin, THE STRESS ANALYSIS OF CRACKS HANDBOOK, Del Research Corporation, Hellertown, Pa., 1973.

4. G.C. Sih, HANDBOOK OF STRESS-INTENSITY FACTORS FOR RESEARCHER AND ENGINEERS, Institute of Fracture and Solid Mechanics, Lehigh University, Bethlehem, Pa., 1973.

5. R.K. McFalls, and L. Tall, A STUDY OF WELDED COLUMNS MANUFACTURED FROM FLAME-CUT PLATES, Welding Journal, Vol. 48, April 1969.

6. G.A. Alpsten, and L. Tall, RESIDUAL STRESSES IN HEAVY WELDED SHAPES, Welding Journal, Vol. 49, March 1970.

7. N. Tebedge, G.A. Alpsten, and L. Tall, MEASUREMENT OF RESIDUAL STRESSES, A STUDY OF METHODS, Friz Engineering Laboratory Report No. 337.8, Lehigh University, Bethlehem, Pa., February 1971.

8. S. Render, MEASUREMENT OF RESIDUAL STRESSES BY THE BLIND HOLE DRILLING METHOD, Photoelastic, Inc., Bulletin TDG-5, 1974.

9. J.M. Barsom, FATIGUE BEHAVIOR OF PRESSURE-VESSEL STEELS, WRC Bulletin 194, Welding Research Council, New York, May 1974.

10. J.M. Barsom, FATIGUE-CRACK GROWTH UNDER VARIABLE-AMPLITUDE LOADING IN A514 GRADE B STEEL, ASTM STP 536, American Society for Testing and Materials, Philadelphia, 1973.

11. T.W. Crooker and D.J. Krause, THE INFLUENCE OF STRESS RATIO AND STRESS LEVEL ON FATIGUE CRACK GROWTH RATES IN 140-Ksi Y_S STEEL, Report of NRL Progress, Naval Research Laboratory, Washington, Dec. 1972.

12. Albert S. Kobayashi, EXPERIMENTAL TECHNIQUE IN FRACTURE MECHANICS, FRACTURE MECHANICS, SESA Monograph No. 1, Society for Experimental Stress Analysis, Westport, Conn. 06880, 1973.

VITA

Lung-Hen Chow was born in Keelung, Taiwan, Republic of China (free China) on February 24, 1958. He graduated from Chung Yuan Christian College of Science and Engineering in June 1980 with a B.S. degree in Mechanical Engineering.

The love and the encouragement from his parents, Jui-Chien Chow and Yu-Hua Chang Chow have given him incentive in his study at Lehigh University.

MICRODEX CORRECTION GUIDE (M-0)

CORRECTION

The preceding document has been re-photographed to assure legibility and its image appears immediately hereafter.

RM 2000

REMINGTON RAND
OFFICE SYSTEMS DIVISION